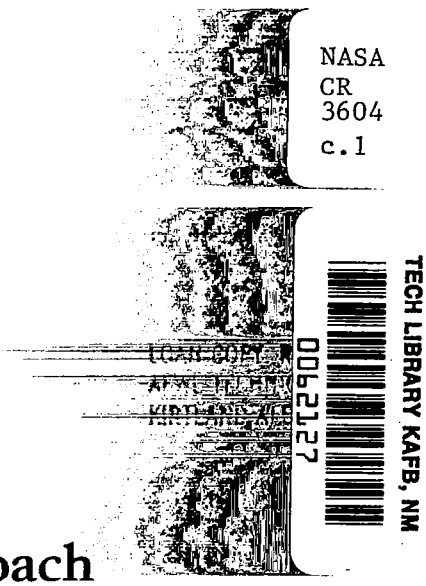

NASA Contractor Report 3604

An Optimal Control Model Approach to the Design of Compensators for Simulator Delay

S. Baron, R. Lancraft,
and A. Caglayan

CONTRACT NAS2-10907
OCTOBER 1982

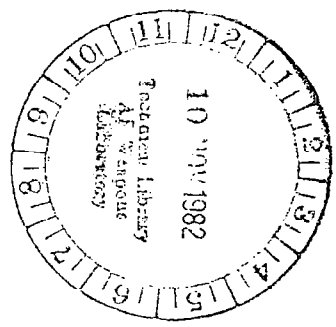

NASA

NASA Contractor Report 3604

An Optimal Control Model Approach to the Design of Compensators for Simulator Delay

S. Baron, R. Lancraft,
and A. Caglayan
Bolt Beranek and Newman Inc.
Cambridge, Massachusetts

Prepared for
Ames Research Center
under Contract NAS2-10907

National Aeronautics
and Space Administration

**Scientific and Technical
Information Branch**

1982

TABLE OF CONTENTS

LIST OF FIGURES

LIST OF TABLES

Abstract

This report summarizes an analytical study of the effects of display delay on pilot performance and workload and of the design of filters to ameliorate these effects. The Optimal Control Model for pilot/vehicle analysis was used both to determine the potential delay effects and to design the compensators. The model was applied to a simple roll tracking task and to a complex hover task. The results confirm that even small delays can degrade performance and impose a workload penalty. A time-domain compensator designed by using the Optimal Control Model directly appears capable of providing extensive compensation for these effects even in multi-input, multi-output problems.

ACKNOWLEDGEMENT

The work reported here was performed under NASA Ames Research Center Contract Number NAS2-10907. The authors wish to thank Mr. Frank Crane, technical monitor for NASA, for his assistance throughout the course of the program.

1. INTRODUCTION

Unwanted delays in digitally-based flight simulators are inherent and arise from the basic sample-data nature of the simulation, the algorithms employed and the lags generated in simulating the appropriate cue environment. With very high-speed, powerful computers used to compute aircraft response, the latter source of delay tends to dominate, particularly with high resolution computer generated imagery being employed. It can be shown theoretically (Baron, Kleinman et al (1970); Baron, Muralidharan and Kleinman (1980)) and has been demonstrated in manual control experiments (Queijo and Reilly (1975); Ricard and Harris (1980); Levison (1979); and Crane (1980)) that the presence of transport delays in wide-band, precision control tasks will degrade performance. Moreover, it is also recognized that, in these situations, delays can increase pilot workload and alter pilot control strategy (Ricard and Harris (1980) and Crane (1980)). For these reasons, it is important to minimize simulation hardware and software delays in the design process and, subsequently, to compensate for any remaining significant delay, if possible.

Of course, the significance of a given simulation delay will depend on the particulars of the simulated flight task, i.e., on the vehicle dynamics, disturbances and control objectives. Moreover, the appropriate form and parameters for a delay

compensation filter will also depend on these factors. These complications, along with the multivariable nature of the flight control problems of prime interest today, make it difficult, if not altogether impractical, to design compensation filters on a "rule-of-thumb" basis. However, developments in pilot modelling suggest that it may be possible to use closed-loop pilot-vehicle models in the design and evaluation of compensation filters for such complex control tasks.

This report describes the results of an analytic study to apply the Optimal Control Model (OCM) for pilot-vehicle analysis to the delay compensation problem. Though the techniques explored and developed are general in nature, the prime focus of the effort is on delays arising in the simulation of precision hover of the Rotor Systems Research Aircraft (RSRA).

The basic, underlying view in the approaches pursued here is that the objective of delay compensation for piloted simulation is to restore the situation, as seen and experienced by the pilot, as closely as possible to that which would be obtained in the absence of unwanted delay. Ideally, delay compensation should restore the performance of the system, as observed by the pilot, to that of the observed performance without delay. In addition, and most importantly, pilot strategy and workload should also be restored to that of the no-delay situation. Because perfect compensation is

not realizable (it requires a pure time advance), one can only hope to accomplish these objectives approximately. A second fundamental idea in our approach is that the best approximation to the no-delay situation is most likely to be arrived at via a suitable closed-loop analysis that considers the pilot explicitly and that this can be achieved with the OCM.

There are, in fact, several ways in which the OCM can be applied to the delay compensation problem. The most obvious application is to predict the effects of delay on the performance of the system and the pilot (including pilot workload). Then, candidate compensation filters can be evaluated using model predictions and the parameters of those filters may be "tuned" to improve their performance. Less obvious is the use of the model for direct design of compensation filters. Two approaches to applying the OCM directly to compensator synthesis are explored herein. Both approaches appear to lead to very effective compensators for single loop problems, particularly for delays on the order of those associated with current CGI systems. However, one of these approaches is easier to apply and generalizes more readily to multivariable systems. It seems highly desirable that this approach be tested empirically.

The report is organized as follows. Chapter 2 contains a review of the OCM. The RSRA hover problem of interest is

formulated and analyzed with the OCM in Chapter 3. Delay compensation methods are developed in Chapter 4. The methods are evaluated for single-loop problems and the most promising approach (mentioned above) is applied to the RSRA problem in Chapter 5. The results are summarized briefly and areas for further research are noted in the last chapter.

2. THE OPTIMAL CONTROL MODEL

The Optimal Control Model (OCM) for pilot/vehicle analysis is central to the effort to analyze the effects of simulator delays on precision control tasks and to our approach to designing compensators to ameliorate those effects. Therefore, to aid the reader who is unfamiliar with this model, a brief description of the OCM is included here. More detailed information concerning the theoretical development of the model may be found in the early references (Baron et al (1970) or Kleinman, Baron and Levison (1971)) and a recent review of model applications and status is provided by Baron and Levison (1980).

The OCM is a closed-loop model which requires a detailed definition of the system to be controlled, the command or disturbance inputs to that system and the displayed outputs available to the pilot for monitoring and control. This model is illustrated in Figure 2.1. Below, we discuss the individual elements of the model.

2.1 System Description

The system dynamics are comprised of the dynamics associated with the controlled element and any dynamics associated with measurement (e.g., sensor dynamics), control (e.g., stick dynamics) and display systems (e.g., flight director dynamics or simulator

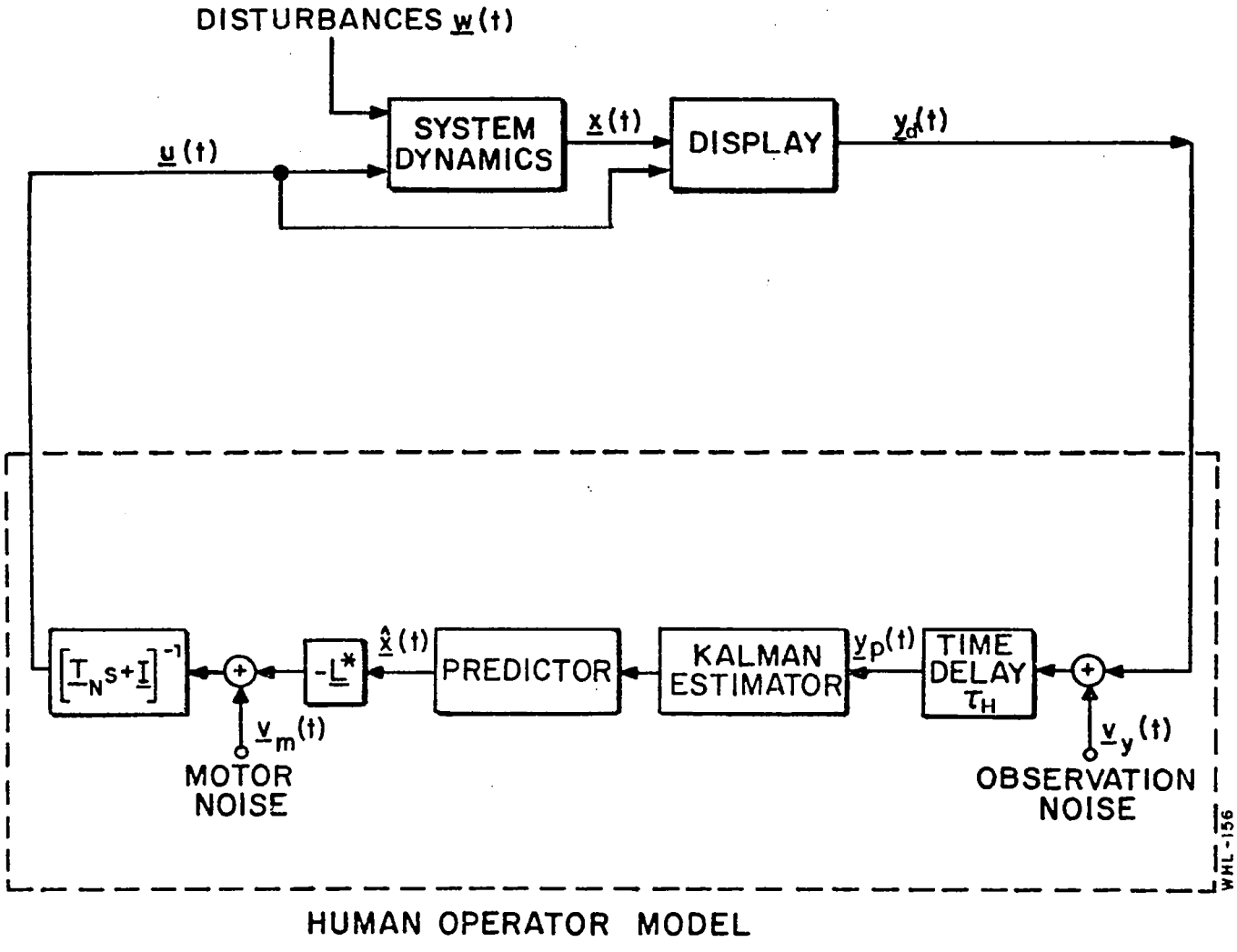

Figure 2.1. Optimal-Control Model for Pilot/Vehicle Systems

drive dynamics). In addition, if system inputs involve time correlations, then these are accounted for by appending appropriate equations to the system dynamics description. For example, in the hover task to be described later, the vehicle is disturbed by random gusts which can be represented by passing white, gaussian noise through appropriate shaping filters; these filters are then included in the system dynamics.

The modelling of the system then involves: a) a linearization of the relevant dynamics associated with each of the subsystems; and b), the construction of a state-variable representation of the combined system dynamics. The resulting vector-matrix state equation has the following form:*

$$\dot{\underline{x}}(t) = \underline{A}\underline{x}(t) + \underline{B}\underline{u}(t) + \underline{E}\underline{w}(t) \qquad (2.1)$$

where $\underline{x}(t)$ is the n-vector which describes the state of the system, $\underline{u}(t)$ the r-vector of pilot control inputs, and $\underline{w}(t)$ a vector of white driving noise processes, the latter included to model the system disturbances. In general, the matrices $\underline{A}$, $\underline{B}$, and $\underline{E}$ may all be time-varying (piece-wise constant) to reflect changes due to differing flight conditions; in the present applications, however, they are fixed for a specific flight condition and vehicle configuration.

*Underscored capital and lower-case letters denote matrices and vectors, respectively.

The display interface provides a means for transforming the system state variables and the pilot's control actions into a display "vector" which represents that set of all information available to the pilot. The components of the display vector are assumed to be linear combinations of the state and control variables, and are defined by the following m-dimensional vector equation:

$$\underline{y}_d(t) = \underline{C}\underline{x}(t-\tau_d) + \underline{D}\underline{u}(t-\tau_d) \qquad (2.2)$$

where $\underline{C}$ and $\underline{D}$ may be time-varying (piece-wise constant) to account for changes in the quantities being displayed or "observed".

As is common practice in applying the OCM, it will be assumed that if a quantity is displayed explicitly to the pilot, he can perceive the rate of change of that quantity. This "implicit" rate-display is then included in the display vector $\underline{y}_d$, along with the actual displayed variables, when performing model analysis.

We have included an explicit indication of any delay, τ_d, associated with the display. For computation, this delay is ultimately "lumped" with the pilot's delay, τ_H, and is, therefore, ignored in most descriptions of the OCM. For the problems studied here, it is useful for discussion purposes to make the separation between display and pilot delay explicit.

For the analyses described later, we will assume that the only information available to the pilot is that which he obtains via his visual and vestibular sensory systems. The display vector $\underline{y}_d$ can be partitioned as follows:

$$\underline{y}_d = (\underline{y}_{vis}, \underline{y}_{ves})^T \tag{2.3}$$

where $\underline{y}_{vis}$ and $\underline{y}_{ves}$ are the sets of output cues provided to the two sensory systems. In the more general situation, the display vector could include "displays" corresponding to other sensory modalities, such as proprioceptive, tactile, or auditory cues. In addition, the individual display vectors associated with a particular modality (e.g., $\underline{y}_{vis}$, $\underline{y}_{ves}$, etc.) can be expanded to account for information provided by other cueing systems which impinge on that same modality. Thus, in the RSRA hover problem to be examined later, we have assumed that $\underline{y}_{vis}$ reflects the pilot's reliance on only out-the-window (visual) cues as provided by the CGI; if he were to have available additional instrument (visual) cues, we would augment $\underline{y}_{vis}$ to account for the information provided by this additional (same-modality) cueing system.

In general, the processing provided by the pilot's sensory systems requires a model which involves not only a linear

transformation of the system state (as in (2.2)), but also a dynamic transformation which accounts for any important sensory processing dynamics (e.g., vestibular dynamics). As noted earlier, this latter modelling requirement would be implemented by assigning the sensory dynamics to the set of overall system dynamics, and appropriately augmenting the state equation of (2.1) (Baron, Lancraft and Zacharias (1980)). However, in the present study, vestibular dynamics were ignored.

2.2 The Pilot Model

The basic assumption underlying the optimal control model for the pilot is that the well-trained, well-motivated human controller will perform in a near optimal manner subject to certain internal constraints that limit the range of his behavior and also subject to the extent to which he understands the objectives of the task. When this assumption is incorporated in the optimal control framework and when appropriate limitations on the human are imposed, the structure shown within the dashed lines of Figure 2.1 results. In discussing this structure it is convenient and meaningful to view this model as being comprised of the following:

(i) an "equivalent" perceptual model that translates the displayed variables into noisy, delayed "perceived" variables denoted by $\underline{y}_p(t)$; (ii) an information processor, consisting of

an optimal (Kalman) estimator and predictor that generates the minimum-variance estimate $\hat{\underline{x}}(t)$ of $\underline{x}(t)$; (iii) a set of "optimal gains", $\underline{L}^*$, chosen to minimize a quadratic cost functional that expresses task requirements; and (iv) an equivalent "motor" or output model that accounts for "bandwidth" limitations (frequently associated with neuromotor dynamics) of the human and his inability to generate noise free controls. We now discuss these model components in greater detail.

2.2.1 Perceptual Model

Limitations on the pilot's ability to process information "displayed" to him are accounted for in the "equivalent" perceptual model. This model translates the displayed variables $\underline{y}_d$ into delayed, "noisy" perceived variables $\underline{y}_p$ via the relation

$$\underline{y}_p(t) = \underline{y}_d(t-\tau_H) + \underline{v}_y(t-\tau_H)$$

$$\underline{y}_p(t) = \underline{C}\underline{x}(t-\tau) + \underline{D}\underline{u}(t-\tau) + \underline{v}_y(t-\tau) \qquad (2.4)$$

where τ_H is an "equivalent" perceptual delay of the pilot, $\tau = \tau_d + \tau_H$ and $\underline{v}_y$ is an "equivalent" observation noise vector.*

* The use of the word equivalent in this context is to emphasize that the parameters may be lumped representations of a variety of limitations that cannot be "identified" separately by existing measurement techniques.

The various internal time delays associated with visual, vestibular, central processing and neuro-motor pathways are combined and conveniently represented by the lumped, equivalent perceptual time delay τ_H. Typical values for this delay are $\emptyset.2 \pm .\emptyset5$ sec. (Kleinman, Baron and Levison (1971)).

The observation noise y_y is included to account for the pilot's inherent randomness, due to random perturbations in human response characteristics, errors in observing displayed variables, and attention-sharing effects which limit the pilot's ability to accurately process all the cues simultaneously available to him. In combination with the motor noise model (described below in section 2.2.3), the observation noise model provides a convenient and accurate means of modelling pilot remnant and thus accounting for random control actions.

For manual control situations in which the displayed signal is large enough to negate the effects of visual resolution ("threshold") limitations, the autocovariance of each observation noise component appears to vary proportionally with mean-squared signal level. In this situation, the autocovariance of the i^{th} output, y_i, may be represented as

$$V_i(t) = \pi P_i \sigma^2_{y_i}(t) \qquad (2.5)$$

where σ^2_{yi} is the variance of the i^{th} output, P_i is the "noise/signal ratio" for the i^{th} display variable, and has units of normalized power per rad/sec. Numerical values for P_i of $\emptyset.\emptyset 1$ (i.e., -2$\emptyset$ dB) have been found to be typical of single-variable control situations (Levison, Elkind and Ward (1971), Kleinman, Baron and Levison (1971)).

The perceptual model defined by (2.4) and (2.5) applies to "ideal" display conditions, in which the signal levels are large with respect to both system-imposed and pilot-associated thresholds. To account for threshold effects we let the autocovariance for each observation noise process be

$$V_i(t) = P_i \left(\frac{\sigma_i^2}{K_i^2(\sigma_i, a_i)} \right) \tag{2.6}$$

where the subscript i refers to the i^{th} display variable. The quantity $K(\sigma_i, a_i)$ is the describing function gain associated with a threshold device

$$K(\sigma, a) = \frac{2}{\sqrt{\pi}} \int_{-\infty}^{\frac{-a}{\sigma\sqrt{\pi}}} e^{-x^2} \, dx \tag{2.7}$$

where "a" is the threshold and σ_i is the standard deviation of the "input" to the threshold device. The net result of this type of describing function model is to increase the observation noise covariance as the display signal variance becomes smaller relative to the threshold.

The sources of these threshold effects depend on the particular task being modelled. They may be associated with the system display implementation, for example, due to resolution limitations on a display screen. Or, they may be associated with the pilot's sensory limitations, such as one might identify with visual acuity thresholds. In the hover task, both types of threshold effects enter into the analysis, as was discussed in detail in Baron, Lancraft and Zacharias (1980).

One additional factor which tends to increase the observation noise (associated with any given display variable) is the pilot's attention-sharing limitations. Because the numerical value associated with the pilot's noise/signal ratio (P_o) has been found to be relatively invariant with respect to system dynamics and display characteristics, we associate this parameter with limitations in the pilot's overall information-processing capability. This association leads to a relatively straightforward model for pilot attention-sharing and workload.

Very briefly, consider that attention-sharing may be required at two levels: between control-related (including monitoring of automatic control performance) and non-control tasks; and among the displays required for performing the control task. For example, a pilot might share attention between control and communication and, while controlling, between flight path and

attitude displays. When motion cues are available, one might also assume that attention is shared between visually-presented display variables as a group and "display" variables supplied by motion sensors. Thus, define

f_t = fraction of attention devoted to the control task as a whole

f_i = fraction of attention devoted to the i^{th} display

Then, the effects of attention-sharing are modelled by an increase in the "nominal" noise/signal ratio, i.e., by

$$P_i = P_o/\left(f_t \cdot f_i\right) \tag{2.8}$$

where P_i is the noise signal ratio associated with the i^{th} display when attention is being shared and P_o is the base, or nominal, noise/signal ratio corresponding to full attention being devoted to the display. The fractional attentions satisfy $f_i \leq 1$ and $\sum_i f_i = 1$. The nominal value for P_o is usually chosen to be equal to .Ø1 (or -2ØdB), which corresponds to the average noise/signal ratio measured in single axis, laboratory tracking tasks in which subjects are highly practiced and motivated (Kleinman, Baron and Levison (1971)); the level of effort involved in these tasks is substantial and a requirement to maintain this level of attention to the manual control task for more than short periods of time

would probably be undesirable or unacceptable in realistic situations.

To predict the effect on specific tasks of sharing attention, model solutions are used to determine the optimum allocation of attention, which, in line with the fundamental optimality hypothesis, is taken as a prediction of the pilot's allocation. This model for task interference has been validated for both control tasks and for monitoring tasks.

In addition to the allocation of attention among display variables (f_i), the model can be used to predict the tradeoff between system performance and attention to the tracking task as a whole (f_t). In this context, the value of f_t necessary to achieve a criterion level of performance is taken to be an indicator of the "attentional workload" of the tracking task.

2.2.2 Estimation and Control Models

The optimal predictor, optimal estimator, and optimal gain matrix represent the set of "adjustments" or "adaptations" by which the pilot tries to optimize his behavior. The general expressions for these model elements are determined by system dynamics and task objectives according to well-defined mathematical rules (Baron, et al (1970), Kleinman, Baron and Levison (1971)). The controller is assumed to adopt a response strategy to minimize a weighted sum of

averaged output and control variances as expressed in the cost functional:

$$J(\underline{u}) = E[\underline{y}^T(t)\underline{Q}_y\underline{y}(t) + \underline{u}^T(t)\underline{Q}_u\underline{u}(t) + \dot{\underline{u}}^T(t)\underline{R}_u\dot{\underline{u}}(t)] \quad (2.9)$$

where $J(\underline{u})$ is conditioned on the perceived information $\underline{y}_p$.* The control gains $\underline{L}^*$ and the "neuro-motor" lag matrix $\underline{T}_N$ (see below) are determined solely by the system matrices (A,B,C,D) and the cost functional weightings.

The selection of the weightings $\underline{Q}_y = \text{diag}\,[q_{y_i}]$, $\underline{Q}_u = \text{diag}\,[q_{u_i}]$ and $\underline{R} = \text{diag}\,[r_i]$ in $J(\underline{u})$ is a non-trivial step in applying the OCM. The most commonly used method for selecting reasonable a priori estimates for the output weightings is to associate them with allowable deviations in the system variables, as has been described in several recent applications of the OCM (see, for example, Kleinman (1976)). The control related weightings may be chosen in a similar fashion or they may be picked to yield a desired value of T_N, as discussed below. This method of choosing weightings has several advantages. Maximum or limiting values of system quantities are often easy to specify or elicit from pilots. In addition, with this normalization, the contribution of each term to the total cost depends on how close that quantity is to its

* The cost functional can also include a term that is quadratic in the state.

maximum value; the penalty is relatively small when the variable is within limits but increases rapidly as the variable exceeds its limit.

As noted above, the tandem of estimator and predictor generate a minimum variance estimate of the system state from the observed data $\underline{y}(s)$, $s \leq t$. As such, they (linearly) compensate for any time delays or noises introduced by the system and/or the operator.

More precisely, the Kalman estimator generates a best estimate $\hat{\underline{x}}(t-\tau)$ of the delayed system state from the observed data, while the predictor, which compensates for the time delay, obtains a least-mean-squared prediction $\hat{\underline{x}}(t)$ from the estimate of the delayed state. Note that the best estimate of the delayed state, $\hat{\underline{x}}(t-\tau)$, is not the best estimate of the state, $\hat{\underline{x}}(t)$, delayed by τ seconds. To avoid confusion we shall set $\underline{p}(t) \triangleq \hat{\underline{x}}(t-\tau)$ in what follows. Both elements of the data reconstructor are dynamic systems that employ models of the actual system. The equation for the estimator is

$$\dot{\underline{p}}(t) = [\underline{A}-\underline{\Sigma C}'\underline{V}^{-1}\underline{C}]\underline{p}(t) + \underline{\Sigma C}'\underline{V}^{-1}\underline{y}(t) + \underline{B}\, u_c(t-\tau) \qquad (2.10)$$

where $\underline{V}$ is the matrix of observation noise covariance and $\underline{\Sigma}$ is the covariance matrix of the estimation error. The error covariance matrix, $\underline{\Sigma}$, is the constant, positive definite solution of the matrix Riccati variance equation associated with the Kalman filter (Baron, et al (1970)). The prediction process is governed by the equations

$$\hat{\underline{x}}(t) = e^{\underline{A}\tau}[\underline{p}(t) - \underline{z}(t-\tau)] \tag{2.11}$$

$$\dot{\underline{z}}(t) = \underline{A}\underline{z}(t) + \underline{B}\underline{u}(t) \tag{2.12}$$

The predictor is particularly important in this study because it includes the "optimal" closed-loop compensation for the display delay. This added compensation helps to explain the increased workload imposed by the delay. More importantly, as will be seen later, the model's predictive compensation can be used to guide the design of a compensator for the simulator delay.

2.2.3 Motor Model

Limitations on the pilot's ability to execute appropriate control actions are accounted for in the motor model, which is composed of a white motor noise source and a first-order lag matrix. This model translates "commanded" controls, $\underline{u}_c$, into the output control actions $\underline{u}$ via the following relation:

$$T_N\dot{\underline{u}} + \underline{u} = \underline{u}_c + \underline{v}_m \tag{2.13}$$

$$\underline{u}_c = \underline{L}^*\hat{\underline{x}}(t)$$

where T_N is an "equivalent" lag matrix and $\underline{v}_m$ is an "equivalent" motor-noise vector.

In laboratory tracking tasks with optimized control sticks, the motor lag parameters have been associated with the operator's

neuro-motor time constant; accordingly, the lag values of the T_N matrix have been set to a value of about Ø.1 second. For more realistic flight control situations, however, this bandwidth limitation may be overshadowed by the system dynamics and flight control objectives, so that the Ø.1 second value may lead to model predictions of control activity which exceed that observed in actual flight situations. In these cases, it is more reasonable to choose lag values by a model trade-off analysis in the following manner: choose a lag value such that if a larger value is chosen, substantial increases in tracking error will result, whereas if a smaller value is chosen, only marginal improvements in tracking performance will result. This method of choosing the motor lag at the "knee" of the cost vs. lag value curve was used for the study of hover described in Baron, Lancraft and Zacharias (1980), the results of which were employed herein.

The neuro-motor noise vector of (2.13) is provided to account for random errors in executing intended control movements, and, in addition, to account for the fact that the pilot may not have perfect knowledge of his own control activity. The motor noise is assumed to be a white noise, with autocovariance that scales with the control variance, i.e.,

$$V_{m_i}(t) = P_{m_i} \sigma^2_{u_i}(t) \qquad (2.14)$$

Previous studies (Kleinman, Baron and Levison (1971)) have found, typically, that a value for P_m of .003 (i.e., a "motor noise ratio" of -25 dB) yields a good agreement with experimental results. Throughout this study the motor-noise ratio was set to approximately -25 dB.

2.3 Model Outputs

A variety of performance measures can be predicted with the OCM and these predictions may be used to evaluate design alternatives in much the same manner as a man-in-the-loop simulation would be used. For the steady-state control tasks of interest here, closed-form expressions are available to compute rms values for any state, output or control variable. Pilot describing functions and remnant spectra that can be measured experimentally (as well as some theoretical describing functions that cannot be measured) are also available from direct computation. In addition, it is possible to obtain derived indicators of pilot workload and vehicle handling quality. In this section, we discuss some of these outputs in terms of the objectives of the present study but do not present the detailed equations used in computing them, which can be found in Kleinman, Baron and Levison (1971).

Performance scores in terms of rms tracking or disturbance regulation errors are available from the OCM. In addition, rms

values for pilot control inputs are predicted and may be used as one measure of manual control workload. It has been shown (Kleinman, Baron and Levison (1971)), that all rms state, output and control scores increase monotonically with time delay τ. For delay times that are short in comparison to system time constants the scores increase linearly with the delay; for larger values of delay the increase becomes exponential. Thus, it is expected that simulation delay will inevitably degrade performance (in terms of tracking or regulation errors) and will increase control workload (unless the pilot is forced to reduce control inputs because of incipient PIO problems arising from the decreased phase margins that result from the delay).

In addition to individual scores, the value of J, the cost functional, is computed. This quantity may be viewed as a convenient scalar metric of overall performance as it combines error and control related scores. Hess (1977) has shown a correlation of J with pilot opinion of vehicle handling qualities under certain reasonable assumptions, thus providing further impetus for using this quantity as a measure of performance.

For a linear, time-invariant system the OCM pilot model can be described in the frequency domain as well as by the time-domain expressions given above. This is accomplished simply by taking the Fourier Transform (or Laplace Transform) of the appropriate equations in Section 2.2. In general terms, one obtains

$$\underline{U}(j\omega) = \underline{H}(j\omega)\underline{Y}_d(j\omega) \tag{2.15}$$

where the capital variables denote the transform of corresponding lower-case variables and where $\underline{H}(j\omega)$ is a matrix of pilot describing functions. Referring to Figure 2.1, the human's describing function can be expressed as

$$\underline{H}(j\omega) = (j\omega T_N + I)^{-1} L^* \underline{P}(j\omega)\underline{E}(j\omega)e^{-j\omega\tau_H} \tag{2.16}$$

where I is the identity matrix and $\underline{P}$ and $\underline{E}$ denote the transfer functions of the predictor and estimator, respectively; i.e.,

$$\hat{\underline{x}}(j\omega) = \underline{P}(j\omega)\ \underline{p}(j\omega) \tag{2.17}$$

$$\underline{p}(j\omega) = \underline{E}(j\omega)\underline{Y}_p(j\omega) \tag{2.18}$$

Expressions for $\underline{P}(j\omega)$ and $\underline{E}(j\omega)$ are determined by substituting (2.13) into (2.10-2.12) and taking the Fourier transform of the resulting equations. Reference to those equations reveals that, because of the closed-loop nature of the task and the fact that $\underline{u}$ is a linear function of $\hat{\underline{x}}(t)$, the predictor transfer function $\underline{P}$ will be a complex matrix function of the system matrices $\underline{A}$ and $\underline{B}$, the total time-delay, τ, and the control gains L^* and T_N. Similarly, the estimator transfer function, defined in the above manner, will depend on all these quantities and, through the estimator gain matrix, on the output matrices $\underline{C}$ and $\underline{D}$, and the noise covariance matrices, $\underline{W}$, $\underline{V}_y$ and $\underline{V}_m$. Thus, overall pilot gain

and phase, as measured by pilot describing functions will depend on all the system variables and all the human limitations, as one should expect.

The matrix of transfer functions $\underline{H}(j\omega)$ are generally not measurable in an experiment and may be thought of as "internal" describing functions. However, the OCM can be used to predict any describing function that is measurable in an experiment (as well as the correlated and uncorrelated spectral components of any variable). Of particular interest is the Equivalent Describing Function, E_{ijk}, defined as the following ratio of cross-power spectral density functions

$$E_{ijk}(j\omega) = \frac{\Phi_{u_i w_k}(j\omega)}{\Phi_{y_i w_k}(j\omega)} \tag{2.19}$$

where w_k signifies the k-th disturbance noise process. This describing function is the one that can most readily be obtained experimentally and, for single loop tasks, corresponds to the usual describing function of classical manual control theory. Inasmuch as the vehicle transfer function is readily computed, one can compute the open-loop describing function as well (i.e., the $Y_p Y_c$ of classical theory) and obtain gain and phase margins, etc.

Unfortunately, in multi-input, multi-output problems the equivalent describing functions are often very difficult to interpret. The unmeasurable internal describing functions, on the other hand, have a fairly direct meaning and have proven useful for flight director design (Levison (1973)) and for design of washout algorithms (Baron, Lancraft and Zacharias (1980)). In the analysis of the RSRA problem later, we shall examine a composite or multiple internal describing function defined as follows. Because we assume that both position and rate of a displayed variable are perceived by the pilot, we can write any row of Eq. (2.15) as

$$u_i = \sum_{k=1,3,5,\ldots} H_{ik} y_j + H_{ik+1} \dot{y}_k$$

$$= \sum_{k=1,3,5,\ldots} (H_{ik} + j\omega H_{ik+1}) y_k$$

where we have assumed the variables in the display vector are ordered in position-rate pairs. The multiple internal describing function between control i and any particular display comprised of variables y_k and $\dot{y}_k$ is then defined as

$$\frac{u_i}{y_k} = H_{ik}(j\omega) + j\omega H_{ik+1}(j\omega) \qquad (2.20)$$

3. THE CLOSED-LOOP RSRA HOVER TASK

The task analyzed here is simulated hover of the RSRA (Rotor System Research Aircraft) over a fixed point at a fixed (low) altitude in the presence of disturbances generated by air turbulence. Control is to be maintained by relying on extra-cockpit visual cues obtained from an out-the-window view and by motion cue associated with helicopter rotation and translation. Visual cueing is assumed to be provided by a computer generated image (CGI) system, and motion cueing by a motion platform. The problem addressed in this analysis was to determine the potential effects of delays in the CGI and motion systems on closed-loop hover performance and pilot workload.

In this chapter, we describe how the task was modelled using the OCM. The model formulation draws extensively on previous modelling studies of hover tasks, particularly on the analysis of Baron, Lancraft and Zacharias (1980). Then, model predictions of the effects of cueing delays on hover performance are presented. The theoretical design of a compensator for the fixed-base version of the task is discussed in a subsequent chapter.

3.1 Description of Control Task

3.1.1 System Dynamics

The RSRA vehicle dynamics were modelled by linearized perturbation equations about a hovering flight equilibrium condition. The equations were written in aircraft body-axes and are shown in Table 3.1. In addition to these equations, expressions to describe the perturbations or "errors" in position about the desired hover point and equations to model the gust disturbances are needed.

The rates of change of position errors $(\dot{x},\dot{y},\dot{z})$ are given by

$$\begin{aligned} \dot{x} &= u\cos\theta_o + w\sin\theta_o \approx u + .115\,w \\ \dot{y} &= v \\ \dot{z} &= -u_o\sin\theta_o + w\cos\theta_o \approx -.115u + w \end{aligned} \tag{3.1}$$

where u,v and w are the perturbation velocities in the x,y and z body-axes, respectively and $\theta_o \sim 6.6$ degrees.

Table 3.1 RSRA Vehicle Dynamics

$\dot{x} = \underline{A}x + \underline{B}u$

$\underline{x}^T = [u\ w\ \Theta\ q\ v\ \phi\ p,\ \psi,\ r]$

$\underline{u}^T = [x_{LONG}\ x_c\ x_{LAT}\ x_r]$

u = perturbation velocity of aircraft in x-body axis, ft/sec

w = perturbation velocity of aircraft in z-body axis, ft/sec

Θ = pitch angle, rad

q = pitch-rate, rad/sec

v = perturbation velocity of aircraft in y-body axis, ft/sec

ϕ = roll angle, rad

p = roll-rate, rad/sec

ψ = yaw angle, rad

r = yaw-rate, rad/sec

x_{LONG} = longitudinal stick deflection, % full scale

x_c = collective stick deflection, % full scale

x_{LAT} = lateral stick deflection, % full scale

x_r = yaw control stick deflection, % full scale

Table 3.1 RSRA Vehicle Dynamics (Cond'd)

VEHICLE DYNAMICS FOR RSRA-HOVER TASK
STATES:U,W,THETA,Q,V,PHI,P,R
CONTROLS:XLONG,XC,XLAT,XR

A MATRIX:

-3.830E-02	9.320E-02	-3.200E+01	1.640E+00	1.510E-03
-4.030E-04	-1.180E+00	-6.440E-01		
1.240E-01	-8.940E-01	-3.740E+00	3.540E-01	-1.180E-02
2.250E+00	-6.200E-01	4.530E+00		
0.	0.	0.	1.000E+00	0.
0.	0.	0.		
1.650E-03	1.920E-03	2.970E-04	-1.750E-01	3.910E-04
6.900E-06	1.130E-01	9.870E-03		
2.160E-02	-1.410E-02	2.640E-01	-1.380E+00	-4.780E-02
3.190E+01	-1.100E+00	1.020E+00		
0.	0.	0.	0.	0.
0.	1.000E+00	0.		
8.790E-03	-4.650E-03	5.860E-04	-1.050E+00	-2.550E-02
8.140E-04	-1.550E+00	1.860E-01		
-3.830E-03	2.170E-03	2.840E-05	-1.280E-03	6.630E-03
-1.830E-04	-3.300E-02	-3.030E-01		

B MATRIX:

1.504E-01	1.404E-01	-2.738E-02	2.616E-03
2.908E-03	-1.122E+00	1.047E-03	-3.315E-04
0.	0.	0.	0.
-1.155E-02	2.618E-03	4.816E-04	-7.356E-05
3.547E-02	1.916E-02	6.188E-02	5.262E-02
0.	0.	0.	0.
7.928E-03	6.938E-03	6.580E-02	1.134E-02
3.031E-05	1.504E-02	2.940E-03	-1.032E-02

The model for gust disturbances was the same as that used by Hoffman, Kleinman and Young (1976) and by Baron, Lancraft and Zacharias (1980) in previous analyses of low altitude hover tasks. The model includes both translational and rotational gusts and requires eight state variables to model the gust spectra which are assumed to be of the Dryden form (Chalk, et al (1969)). Intensities for the gust components were chosen to be

$$\sigma_{u_g} = \sigma_{v_g} = 6.26 \text{ ft/s}$$
$$\sigma_{w_g} = 2.71 \text{ ft/s}$$
$$\sigma_{q_g} = .0177 \text{ r/s}$$
$$\sigma_{p_q} = .0261 \text{ r/s}$$
$$\sigma_{r_g} = .0304 \text{ r/s}$$

According to Chalk et al (1969), these values for wind intensity will be exceeded only about one-third of the time, so the turbulence may be considered to be moderately severe.

The gust equations and the error equations (Eq. 3.1) are appended to the vehicle dynamics of Table 3.1 to obtain the "system dynamics" for application of the OCM. The full set of state-equations, the first eight of which describe the gusts, is given in Table 3.2, where the matrix definitions correspond to the notation used in Eq. (2.1). As can be seen, the full set of equations involves twenty state variables and, therefore,

Table 3.2. RSRA System Dynamics

RSRA DYNAMICS
STATES:UG,WG,WG1,QG,VG,VG1,PG,RG,U,W,THETA,Q,V,PHI,P,R,PSI,X,Y,Z
CONTROLS:XLONG,XC,XLAT,XR

A MATRIX:

-4.740E-02	0.	0.	0.	0.
0.	0.	0.	0.	0.
0.	0.	0.	0.	0.
0.	0.	0.	0.	0.
0.	-5.060E-01	2.530E-01	0.	0.
0.	0.	0.	0.	0.
0.	0.	0.	0.	0.
0.	0.	0.	0.	0.
0.	-2.530E-01	0.	0.	0.
0.	0.	0.	0.	0.
0.	0.	0.	0.	0.
0.	0.	0.	0.	0.
0.	-4.000E-03	2.000E-03	-2.010E-01	0.
0.	0.	0.	0.	0.
0.	0.	0.	0.	0.
0.	0.	0.	0.	0.
0.	0.	0.	0.	-9.480E-02
4.740E-02	0.	0.	0.	0.
0.	0.	0.	0.	0.
0.	0.	0.	0.	0.
0.	0.	0.	0.	-4.740E-02
0.	0.	0.	0.	0.
0.	0.	0.	0.	0.
0.	0.	0.	0.	0.
0.	0.	0.	0.	0.
0.	-2.000E-01	0.	0.	0.
0.	0.	0.	0.	0.
0.	0.	0.	0.	0.
0.	0.	0.	0.	1.000E-03
-5.000E-04	0.	-2.680E-01	0.	0.
0.	0.	0.	0.	0.
0.	0.	0.	0.	0.

Table 3.2. RSRA System Dynamics (Cont'd)

3.830E-02	-9.320E-02	0.	-1.640E+00	-1.510E-03
0.	1.180E+00	6.440E-01	-3.830E-02	9.320E-02
-3.200E+01	1.640E+00	1.510E-03	-4.030E-04	-1.180E+00
-6.440E-01	0.	0.	0.	0.
-1.240E-01	8.940E-01	0.	-3.540E-01	1.180E-02
0.	6.200E-01	-4.530E+00	1.240E-01	-8.940E-01
-3.740E+00	3.540E-01	-1.180E-02	2.250E+00	-6.200E-01
4.530E+00	0.	0.	0.	0.
0.	0.	0.	-1.000E+00	0.
0.	0.	0.	0.	0.
0.	1.000E+00	0.	0.	0.
0.	0.	0.	0.	0.
-1.650E-03	-1.920E-03	0.	1.750E-01	-3.910E-04
0.	-1.130E-01	-9.870E-03	1.650E-03	1.920E-03
2.970E-04	-1.750E-01	3.910E-04	6.900E-06	1.130E-01
9.870E-03	0.	0.	0.	0.
-2.160E-02	1.410E-02	0.	1.380E+00	4.780E-02
0.	1.100E+00	-1.020E+00	2.160E-02	-1.410E-02
2.640E-01	-1.380E+00	-4.780E-02	3.190E+01	-1.100E+00
1.020E+00	0.	0.	0.	0.
0.	0.	0.	0.	0.
0.	-1.000E+00	0.	0.	0.
0.	0.	0.	0.	1.000E+00
0.	0.	0.	0.	0.
-8.790E-03	4.650E-03	0.	1.050E+00	2.550E-02
0.	1.550E+00	-1.860E-01	8.790E-03	-4.650E-03
5.860E-04	-1.050E+00	-2.550E-02	8.140E-04	-1.550E+00
1.860E-01	0.	0.	0.	0.
3.830E-03	-2.170E-03	0.	1.280E-03	-6.630E-03
0.	3.300E-02	3.030E-01	-3.830E-03	2.170E-03
2.840E-05	-1.280E-03	6.630E-03	-1.830E-04	-3.300E-02
-3.030E-01	0.	0.	0.	0.
0.	0.	0.	0.	0.
0.	0.	0.	0.	0.
0.	0.	0.	0.	0.
1.000E+00	0.	0.	0.	0.

Table 3.2. RSRA System Dynamics (Concl'd)

0.	0.	0.	0.	0.
0.	0.	0.	1.000E+00	1.160E-01
0.	0.	0.	0.	0.
0.	0.	0.	0.	0.
0.	0.	0.	0.	0.
0.	0.	0.	0.	0.
0.	0.	1.000E+00	0.	0.
0.	0.	0.	0.	0.
0.	0.	0.	0.	0.
0.	0.	0.	-1.160E-01	1.000E+00
0.	0.	0.	0.	0.
0.	0.	0.	0.	0.

B MATRIX:

0.	0.	0.	0.
0.	0.	0.	0.
0.	0.	0.	0.
0.	0.	0.	0.
0.	0.	0.	0.
0.	0.	0.	0.
0.	0.	0.	0.
0.	0.	0.	0.
1.504E-01	1.404E-01	-2.738E-02	2.616E-03
2.908E-03	-1.122E+00	1.047E-03	-3.315E-04
0.	0.	0.	0.
-1.155E-02	2.618E-03	4.816E-04	-7.356E-05
3.547E-02	1.916E-02	6.188E-02	5.262E-02
0.	0.	0.	0.
7.928E-03	6.938E-03	6.580E-02	1.134E-02
3.031E-05	1.504E-02	2.940E-03	-1.032E-02
0.	0.	0.	0.
0.	0.	0.	0.
0.	0.	0.	0.
0.	0.	0.	0.

E MATRIX:

0.	0.	1.926E+00	0.
0.	0.	0.	2.358E+00
0.	0.	0.	1.362E+00
0.	0.	0.	1.870E-02
2.360E+00	0.	0.	0.
1.360E+00	0.	0.	0.
0.	1.650E-02	0.	0.
-2.480E-02	0.	0.	0.
0.	0.	0.	0.
0.	0.	0.	0.
0.	0.	0.	0.
0.	0.	0.	0.
0.	0.	0.	0.
0.	0.	0.	0.
0.	0.	0.	0.
0.	0.	0.	0.
0.	0.	0.	0.
0.	0.	0.	0.
0.	0.	0.	0.

represents a fairly complex OCM modelling problem. Moreover, because the coupling between lateral and longitudinal axes is likely to be important, these axes will not be considered separately, as is often done to reduce modelling complexity.

3.1.2 Display Variables

Visual display variables were chosen as in Baron, Lancraft and Zacharias (1980). Thus, it was assumed that information concerning the vehicle position errors and error-rates and its attitude and attitude-rate were available from the visual scene generated by the CGI. The visual display vector is then given by

$$\underline{Y}_{vis} = \{x, \dot{x}, y, \dot{y}, z, \dot{z}, \theta, \dot{\theta}, \phi, \dot{\phi}, \psi, \dot{\psi}\} \qquad (3.2)$$

Visual thresholds for these variables were chosen to correspond to the nominal, high resolution CGI configuration of the above reference. The values for these thresholds are given below in the delineation of parameters of the OCM pilot model.

Motion cueing was treated on a strict informational basis with the effects of vestibular dynamics being ignored and with motion platform phase lags lumped into display delays. These assumptions reduce computational complexity and cost and appear to be easily justified in this study with its focus on compensation for display delays (rather than on, say, the design of washout circuits for a motion platform). The display-vector of motion cues is given by

$$Y_{mot} = \{\ddot{x}, \ddot{y}, \ddot{z}, \dot{\theta}, \ddot{\theta}, \dot{\phi}, \ddot{\phi}, \dot{\psi}, \ddot{\psi}\} \quad (3.3)$$

Note that we have assumed that $q \approx \dot{\theta}$, $p \approx \dot{\phi}$ and $r \approx \dot{\psi}$.

3.1.3 Simulator Delays

We assume that both the nominal main-frame sampling frequency and the CGI refresh rate are 30 Hz. This results in a nominal visual path delay of .132 seconds (Baron, Lancraft and Zacharias, 1980).

The motion path delay is composed of the computational delay and the phase lag due to motion dynamics. Using the second-order VMS motion platform dynamics given in Baron, Lancraft and Zacharias (1980) results in motion cue delays of .125 seconds for the y- and z-axis motions and .2 seconds for the x-axis and the rotational motions.

To simplify the analysis, we will assume that the visual and motion delays are equal and will compute performance for a range of delays from .066-.2 seconds, with a nominal delay of .132 seconds.

3.1.4 Cost Functional

The precision hovering task is a disturbance regulation task and, as described in Chapter 2, in applying the OCM, it is assumed that the objectives of the task may be characterized in terms of

the minimization of a quadratic cost functional of output and control variables (Eq. 2.9). The weightings used in this study are

Table 3.3 Cost Functional Weightings

VARIABLE	WEIGHTING
x,y,z	$(1/\ 5\ \text{ft}\ )^2$
u,v,w	$(1/\ 1\ \text{ft/s})^2$
ϕ,Θ,ψ	$(57.3\ /\ 1\ \text{deg})^2$
p,q,r	$(57.3\ /\ .5\ \text{deg})^2$
x_{LONG},x_c,x_{LAT},x_r	$(1\ /\ 100\%)^2$
$\dot{x}_{LONG}$	$(1/12.9\ \%/\text{s})^2$
$\dot{x}_c$	$(1/14\ \%/\text{s})^2$
$\dot{x}_{LAT}$	$(1/11.5\ \%/\text{s})^2$
$\dot{x}_r$	$(1/14\ \%/\text{s})^2$

given in Table 3.3. The weightings on outputs are the same as in Baron, Lancraft and Zacharias (1980) and those on control-rate activity yield the same neuro-motor time constants for this problem as were used in that reference (see below). It should be noted that the "limits" corresponding to these weightings are very

optimistic for the task and level of wind. This will result in large values of J. However, if all weightings are multiplied by the same scale factor, there will be no change in performance or strategy other than a reduction in the value of J.

3.2 Parameters of OCM Model of the Pilot

Pilot time delay and motor noise/signal ratio were set at their nominal values of .2 seconds and -25 dB, respectively. As noted earlier, neuro-motor time constants for the four controls were chosen to be the same as in the study of Baron, Lancraft and Zacharias (1980); the values used were

longitudinal controls: T_N = [.15 sec, .18 sec]

lateral controls: T_N = [.1 sec, .1 sec]

As in previous studies, a value of -20 dB was selected for the observation noise/signal ratio corresponding to unity attention to the control task. Then, overall attention to the task was used as a parameter of the analysis to explore possible workload effects. For a given level of attention to the total control task, fractional attentions to individual displays were optimized; that is, they were selected to minimize the performance index J.

Visual and motion perceptual thresholds were also set equal to the values derived in Baron, Lancraft and Zacharias (1980) and are given in Table 3.4.

Table 3.4 Perceptual Thresholds*

Variable	Visual	Motion Platform
x, ft	.84	--
$\dot{x}$, ft/sec	.21	--
y, ft	.04	--
$\dot{y}$, ft/sec	.17	--
z, ft	.37	--
$\dot{z}$, ft/sec	.10	--
$\ddot{x}$, ft/sec^2	--	.053
$\ddot{y}$, ft/sec^2	--	.053
$\ddot{z}$, ft/sec^2	--	.053
θ, deg	.05	--
q, deg/sec	.20	3.6
$\dot{q}$, deg/sec^2	--	.67
ϕ, deg	.02	--
p, deg/sec	.09	2.5
$\dot{p}$, deg/sec^2	--	.41
ψ, deg	.05	--
r, deg/sec	.20	4.2
$\dot{r}$, deg/sec^2	--	.41

* An entry of -- means that it is assumed that no information on the variable is provided by the modality

3.3 Results

In this section, the OCM predictions of the effects of delay on total performance J, hover error $R = \sqrt{x^2+y^2+z^2}$, and workload are presented. In addition, although not a principal concern in the present study, the effects of providing motion cues are also analyzed.

The effect of delay on performance is shown in Figure 3.1 for both fixed-base and motion conditions. The results are for unity attention (P_o=-20dB, f_t=1) to the control task. Note that the effect on J is accentuated relative to that on R partly because J is like an error squared. Clearly, adding display delay degrades performance. The increase in J due to the introduction of a delay of .132 seconds is about 30% for both fixed-base and motion-base conditions. The corresponding increase in hover error is about 20% for the fixed-base condition and 25% for the motion-base condition. Figure 3.1 also shows that performance is better when motion cues are available, for the range of delay values considered here; indeed, in this range, fixed-base performance measures are almost 50% higher than corresponding motion-base measures.

To provide a somewhat more detailed look at the effect of delay on performance, individual output and control scores are given in Table 3.5. All variables show the same trends evidenced in Figure 3.1, as expected. It is interesting to note that

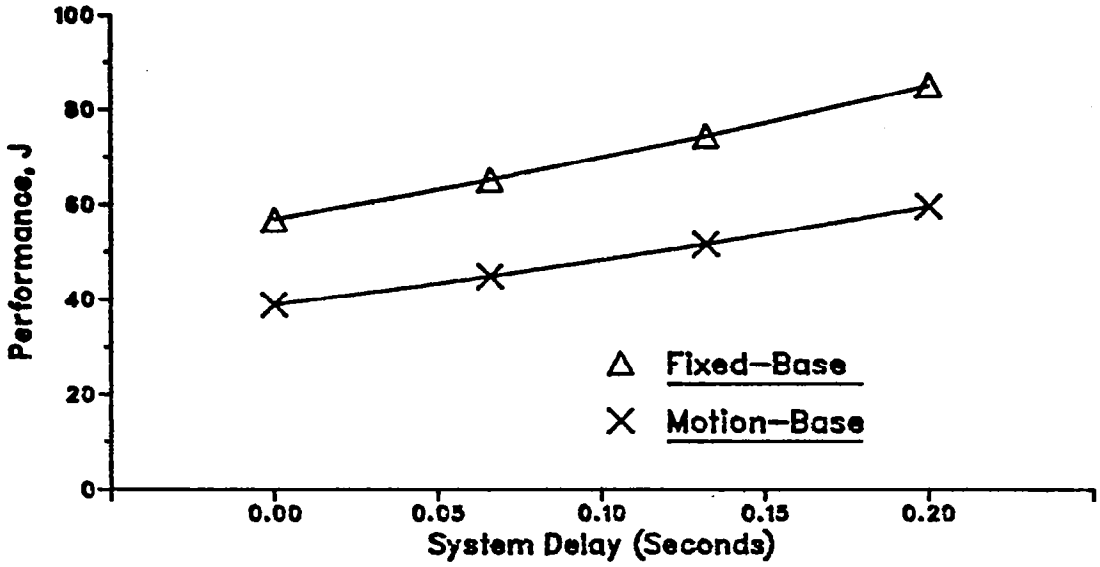

FIGURE 3.1a: EFFECT OF SYSTEM DELAY ON PERFORMANCE

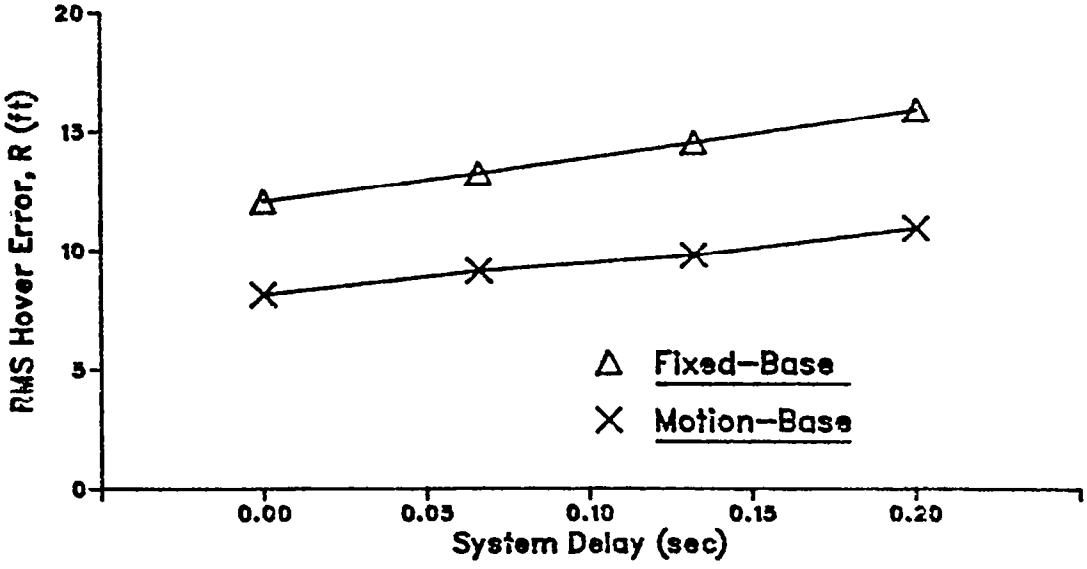

FIGURE 3.1b: EFFECT OF SYSTEM DELAY ON RMS HOVER ERROR

Table 3.5 Effect of Delay on RMS Outputs and Control Scores

	FIXED-BASE		MOTION BASE	
VARIABLE	DELAY=0 SEC	DELAY=.132 SEC	DELAY=0SEC	DELAY=.132 SEC
x, ft	8.47	9.87	5.79	6.96
y, ft	7.48	9.87	4.92	6.58
z, ft	3.86	4.49	2.73	3.48
θ, deg	1.53	1.75	1.12	1.32
ϕ, deg	1.43	1.79	1.05	1.37
ψ, deg	0.99	1.29	0.73	0.97
X_{LON}, %	3.73	4.05	3.22	3.53
X_C, %	2.38	2.38	2.33	2.35
X_{LAT}, %	2.25	2.30	2.20	2.25
X_r, %	7.38	7.86	6.95	7.40

performance with delayed visual and motion cues is slightly better than that predicted for fixed-base simulation with no delay.

As suggested elsewhere in this report and in other references (e.g., Crane, 1980), delay is expected to increase pilot workload. Figure 3.2 presents performance/workload trade-off curves as a function of cueing condition and delay. Both J and hover error are shown and results are given for the zero delay and nominal delay cases. The ordering of performance as a function of delay and motion condition is seen to hold at all levels of pilot attention. Also, as expected, performance improves with increased pilot attention.

To interpret Figure 3.2 in terms of pilot-workload, we must select a criterion level, J_c. For example, if we select a criterion level about $J_c \sim 56$ as shown in Figure 3.2a (the value for the no-delay, motion-base condition, with a relative attention of .5), we see that the added delay, in the motion case, requires that the pilot devote almost twice the attention to the task in order to achieve the same performance. Interestingly, about the same workload penalty is imposed if motion cues are removed, but no display delay is added. For the fixed-base conditions, achieving the same criterion level requires more than a doubling of

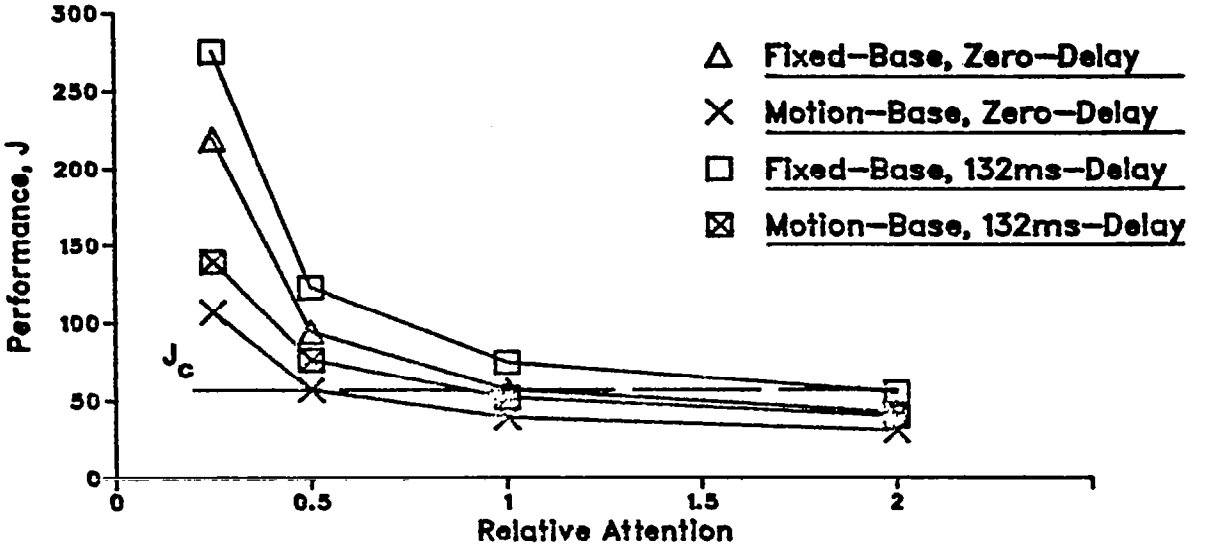

FIGURE 3.2a: EFFECT OF RELATIVE ATTENTION ON PERFORMANCE

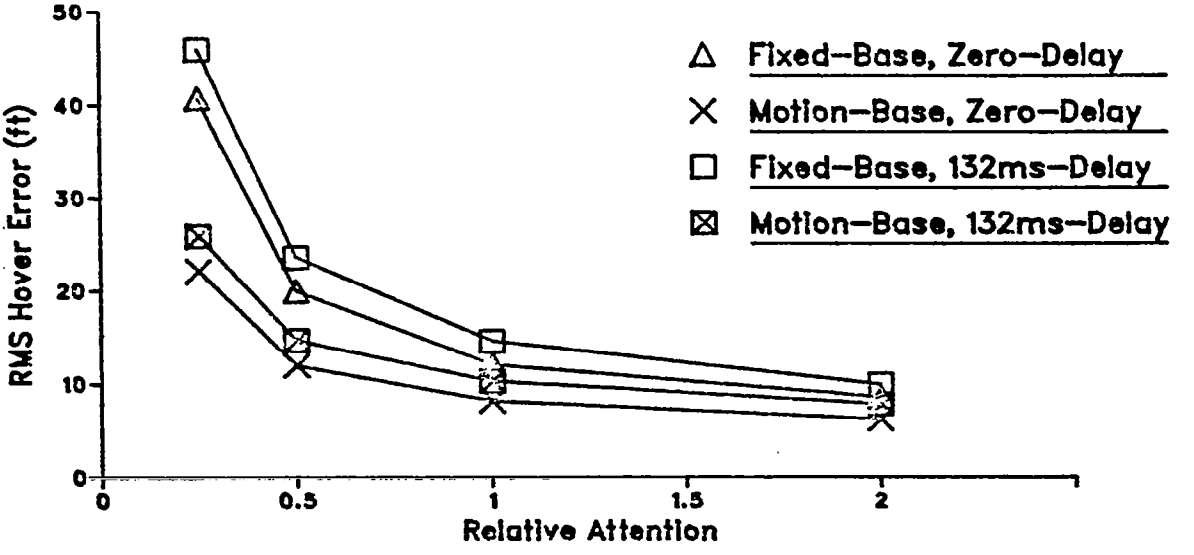

FIGURE 3.2b: EFFECT OF RELATIVE ATTENTION ON RMS HOVER ERROR

attention, if this performance level can be achieved at all.*

If workload is explored in terms of hover error (Figure 3.2b) we get similar results. For a criterion error of ten feet to be maintained for the motion-base cases, attention must be increased from ≈.58 to almost 1 when delay is added. For the fixed-base condition, if fifteen feet is chosen as criterion performance, then the relative attention must increase from about .7 for zero delay to about .86 for .132 seconds of delay.

The results in Figure 3.2 show that, regardless of the criterion level selected, the introduction of simulator delay requires that the pilot devote significantly more attention to the task if performance is to be maintained at the zero-delay level. Alternatively, the pilot can maintain the same level of attention or increase it to a lesser degree, but with degraded performance. Inasmuch as both performance and workload affect pilot opinion, it is clear that delays will bias that opinion in the direction of poorer ratings for vehicle handling qualities.

In addition to the above results, "internal" pilot describing functions were computed. These describing functions are shown later in Chapter 5 where the effects of delay compensation are

---

* Computations were not carried out for relative attentions > 2 and it is not clear where the fixed-base, delay curve asymptotes.

examined. Briefly, the internal describing functions indicate an increase in pilot lead with added display delay, as expected.

4. COMPENSATOR DESIGN

In this chapter, the design of compensators for simulator delay is addressed. First, the design objectives are discussed from a "pilot-centered" viewpoint. Then, three approaches to compensator design are presented. One approach, proposed in the literature (Crane, (1980, 1981)) is based on classical control ideas. The other two approaches, which were developed in this study, are based on the OCM.

4.1 Objectives of Compensator Design

The display compensation problem is illustrated in Figure 4.1. In part (a) of the figure, a no-delay or "baseline" configuration for the simulator is shown. The display "transforms" vehicle state information, $\underline{x}$, into outputs that are used by the pilot to control the aircraft, without adding unwanted delay. For example, a CGI might have helicopter position and attitude as inputs and generate an appropriate "scene" for the pilot to view in attempting to control helicopter position. The outputs, $\underline{y}$, would be the visual cueing information obtained by the pilot from the scene. If the vehicle and scene are modelled faithfully, this "simulation" would be a good representation of actual flight (at least, insofar as it goes). The matrix transfer function between output $\underline{y}$ and control input $\underline{u}$ for the baseline configuration is denoted by $\underline{S}(j\omega)$.

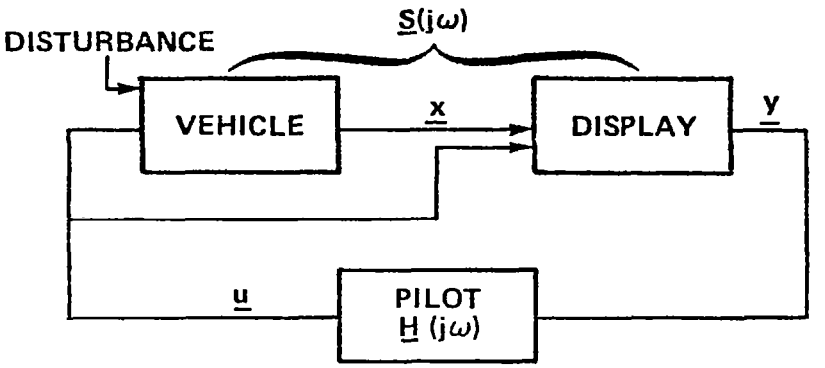

a) No-delay

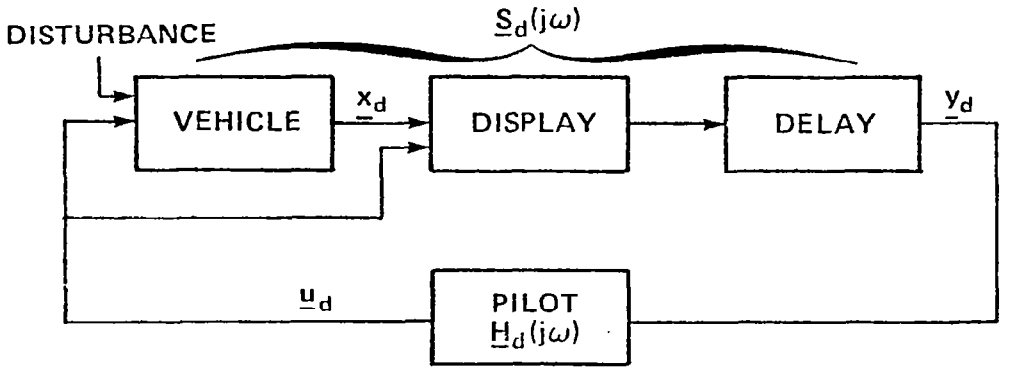

b) Full delay condition

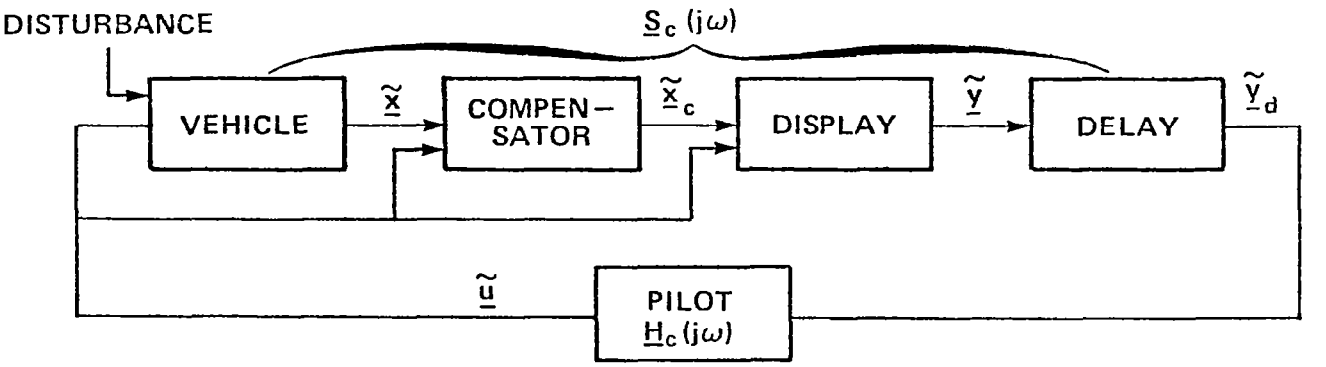

c) Compensated condition

Figure 4.1. Illustration of Delay Compensation Problem

In part (b) of the figure, a delay is added to account for computing and update time for display presentation. As seen by the pilot, the system to be controlled includes this delay and has a transfer function of $\underline{S}_d(j\omega)=\underline{S}(j\omega)e^{-j\omega\tau_d}$. It is known (see, e.g., Ricard and Harris (1980) or Crane (1980)) that the addition of the delay will degrade closed-loop performance when the task for the pilot is a precision control task (such as target tracking, air-to-air refueling, precision hover, etc.). Moreover, the trained pilot will adopt a control strategy, $\underline{H}_d(j\omega)$, that is appropriate for the modified system and different from the strategy, $\underline{H}(j\omega)$, he would use if there was no delay. In general, the modified system will impose a higher workload and, as noted elsewhere, if the pilot is asked to "rate" the handling qualities of the aircraft, he will be biased toward poorer ratings by these factors. The increased workload is usually attributed to a requirement for the pilot to generate lead compensation in the presence of the extra delay. For single-loop control problems, this requirement is readily interpreted in terms of loop phase margin and/or changes in pilot lead as evidence in the open-loop and pilot describing functions.

Figure 4.1c illustrates the compensated simulation. This diagram is more general than, and different from, that normally shown in past references in that the vector-state of the vehicle,

$\underline{x}(t)$, and the pilot's control inputs, $\underline{u}(t)$, are both assumed to be available as inputs to the compensator. This is a reasonable assumption in a simulator environment and is a crucial one for one of the approaches discussed below. For the pilot, the system to be controlled, with a matrix transfer function denoted by $\underline{S}_c(j\omega)$, now includes the compensator and the delay as well as the simulated vehicle. Again, the pilot will adapt his control strategy, as indicated by the modified describing function $\underline{H}_c(j\omega)$.

Now, the basic objective of delay compensation is to obtain performance and pilot response that are as close as possible to that of the no-delay (or baseline) condition. Clearly, if we could implement a compensator with the transfer function $\underline{F}=\underline{I}e^{j\omega\tau_d}$, then we would obtain $\underline{S}_c(j\omega)=\underline{S}(j\omega)$ and the objective would be accomplished. This is not possible because this compensator is unrealizable, but it suggests that one way to approach the compensator design problem is to choose a compensator $\underline{F}$ such that

$$\underline{S}_c(j\omega) \approx \underline{S}(j\omega) \tag{4.1}$$

that is, so that the open-loop transfer function for the compensated system (excluding the pilot) approximates the no-delay transfer function. To find an $\underline{F}$ such that Eq. (4.1) is satisfied in an appropriate fashion is, in the general multivariable case, a very complex approximation problem. One of the major difficulties

is in defining a suitable approximation error in terms of both differential weighting of errors in the various individual transfer functions and of errors at different frequencies.

One straightforward way to attempt to achieve (4.1) is to have the compensator approximate a pure lead. This can be done by using a Taylor series expansion, yielding

$$\underline{E}(j\omega) = I(1+j\omega\tau_d+\ldots) \approx Ie^{j\omega\tau_d} \qquad (4.2)$$

The order of the compensator would be a design parameter that depended on the size of the delay and the availability of derivative information. A major problem with the approach is that it is known to have unacceptable noise amplification properties and, therefore, $\underline{E}$ must be modified to include some noise filtering. The introduction of the noise filter may complicate the compensator design problem (see below).

The above approaches focus on the simulator transfer function and are open-loop in nature. The view that we are proposing in evaluating delay compensators and in the OCM-based design approaches is closed-loop in nature and is pilot-oriented. Thus, we seek a compensator that restores performance and workload (as defined below) as closely as possible to the no-delay case and which yields

$$\underline{H}_c(j\omega) \sim \underline{H}(j\omega). \tag{4.3}$$

Equation (4.3) states that the compensator should result in a pilot describing function that approximates that which would be obtained in the no-delay case. One would expect that picking $\underline{F}$ to satisfy Eq. (4.1) would automatically lead to Eq. (4.3) being satisfied. However, as noted above, open-loop considerations may not, in themselves, reveal what is a good approximation for the closed-loop problem. By focussing on the approximation in Eq. (4.3), we hope to pick a compensator that accomplishes (4.1) in the appropriate closed-loop sense. Of course, to do this effectively and conveniently, one must have an adequate model of the pilot.

The question of what is meant by the restoration of "performance" is somewhat more complicated than might be expected. To simplify the discussion, let $\underline{y}=\underline{x}$ in Figure 4.1; i.e., assume the vehicle-state is displayed. Here, the position taken is that performance, as seen by the pilot, should be restored. In terms of the notation of Figure 4.1, we desire

$$\left(\overline{\underline{\tilde{y}}_d\underline{\tilde{y}}_d'}\right)^{1/2} \approx \left(\overline{\underline{y}\underline{y}'}\right)^{1/2} \tag{4.4}$$

$$\left(\overline{\underline{\tilde{u}}\underline{\tilde{u}}'}\right)^{1/2} \approx \left(\overline{\underline{u}\underline{u}'}\right)^{1/2} \tag{4.5}$$

where the overbar denotes the expected value. Inasmuch as the delay does not change the mean-squared (or rms) value, Eq. (4.4) is equivalent to

$$\left(\overline{\underset{\sim}{x}_c \underset{\sim}{x}_c'}\right)^{1/2} \approx \left(\overline{\underset{\sim}{y}\underset{\sim}{y}'}\right)^{1/2} = \left(\overline{\underset{\sim}{x}\underset{\sim}{x}'}\right)^{1/2} \tag{4.6}$$

Note that this is <u>not</u> the same as requiring

$$\left(\overline{\underset{\sim}{x}\underset{\sim}{x}'}\right)^{1/2} = \left(\overline{\underset{\sim}{x}\underset{\sim}{x}'}\right)^{1/2} \tag{4.7}$$

and, in this view, the compensator and delay are thought of as part of the simulated "vehicle". The criterion embodied in Eq. (4.4) is justified on the basis that it is the meaningful one as far as the pilot is concerned because it deals with quantities he will observe. However, the criterion could lead to anomalous results, if it were not taken in conjunction with the requirements of Eqs. (4.3), (4.5) and, in some measure, (4.1). For example, setting $\underline{F}$ equal to a matrix of simple scale factors could potentially satisfy Eq. (4.6) without resulting in a better simulation.

Finally, the examination of restoration of pilot workload will be based on either or both of two indicators. First, where appropriate, we will consider the classical notion of relating pilot lead in the neighborhood of system crossover frequency to workload. Thus, if the compensator reduces the lead requirements nearly to those of the no-delay case, we will consider that it is resulting in a workload that is approximately the same as for that case. The second approach will be to determine whether no-delay performance can be achieved in the compensated case with the same level of attention as in the no-delay case.

In summary, the design criteria that will be employed in evaluation of delay compensators are picked such that, if satisfied, the situation as seen by the pilot will be restored essentially to that of the no-delay case. Both frequency domain (describing functions) and time-domain (performance scores) criteria are considered along with indicators of pilot workload. It is of course expected that the design goals cannot be achieved completely.

4.2 Classical Compensator

Recent references (Ricard and Harris (1980) and Crane (1980,1981)), have suggested compensating for simulator delay by simple lead-lag filters. These compensators are designed to operate with a single input variable and have a single output; their design is best understood in the simplified single-loop context of Figure 4.2. The frequency response of the lead-lag compensator is given by

$$F_c(j\omega) = K\left(\frac{j\omega T_1+1}{j\omega T_2+1}\right) \tag{4.8}$$

The design problem is to choose the lead and lag time constants, T_1 and T_2, and the gain factor, K, to achieve compensator objectives.

Ricard and Harris (1980) suggest setting the lead time constant, T_1, equal to the delay. Then, T_2 is chosen to yield

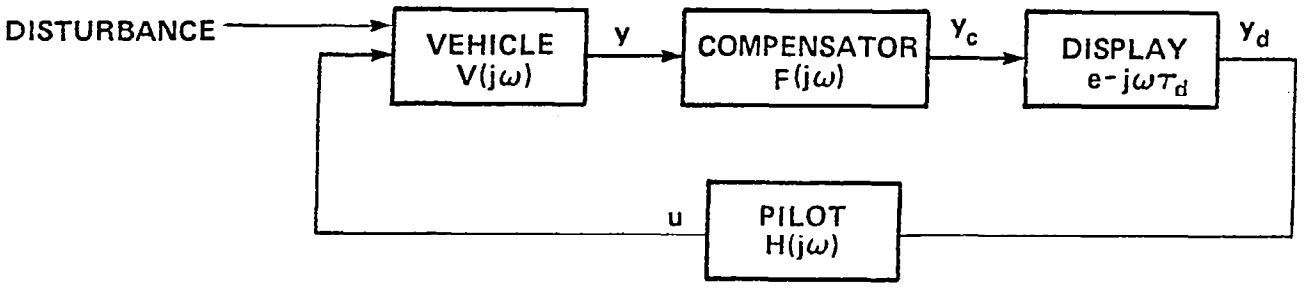

Figure 4.2. Structural Diagram of Single-Loop Delay Compensation

optimal performance. This approach is essentially motivated by an attempt to approximate the pure lead, while filtering unwanted noise. However, the method of selecting T_2, i.e., to obtain the best performance, is inconsistent with the design criterion employed here which is to restore performance to the no-delay case. Therefore, we will not consider this approach further.

An alternative approach to the design of the lead-lag compensator, based on classical, closed-loop control concepts, was proposed by Crane (1980). The basic idea is to pick the time constants to restore the closed-loop phase margin to that of the no-delay case. It is assumed that this will mitigate the need for the pilot to generate the added lead required because of the delay and, thereby, will help alleviate the performance and workload

penalties normally accompanying the delay. The result of a classical control system analysis leads to choosing the design parameters according to (Crane (1980,1981))

$$T_1 \approx \omega_c^+ \tag{4.9a}$$

$$\tan^{-1}\omega_c T_2 = (\tan^{-1}\omega_c T_1) - \omega_c \tau_d \tag{4.9b}$$

$$K = \left|\frac{j\omega_c T_2 + 1}{j\omega_c T_1 + 1}\right|^{1/2} \tag{4.9c}$$

where ω_c is the system crossover frequency, ω_c^+ denotes a frequency slightly higher than ω_c and $|.|$ denotes the magnitude squared. In other words: a) the filter zero is placed slightly beyond crossover; b) the filter pole is chosen so that filter lead cancels the phase lag at crossover due to the delay; and c) the gain factor is chosen to yield unity gain at crossover.

Inasmuch as ω_c depends on pilot strategy, this design method is based on closed-loop criteria. However, one must either measure ω_c in an experiment in which there is no delay, as was done by Crane, or one must have a method for predicting ω_c (i.e., a pilot model). In general, it will not be possible to measure ω_c for a no-delay configuration in other than a laboratory situation; otherwise, one could have a no-delay simulation. Therefore, the use of a pilot model is indicated.

One must note that a basic problem with this classical control system design of the lead-lag network exists in multi-loop situations. For these cases, the appropriate design criteria are far more difficult to specify. For example, for a CGI system, driven by vehicle positions and attitudes, it is not at all clear as to how to apply this approach to compensation of the display inputs. This is particularly true for highly coupled and interacting vehicle dynamics, such as those of a hovering helicopter.*

We will evaluate this approach to compensator design for a single-loop disturbance regulation problem. However, we will modify the design procedure slightly by letting the lead time constant be a parameter of the design that is chosen, via OCM analysis, to restore performance to the no-delay case. The remaining two parameters will then be selected to satisfy equations (4.9b) and (4.9c).

4.3 OCM Frequency Domain Compensator

It was pointed out in Chapter 2 that the OCM contains a predictor that compensates optimally for the pilot's inherent delay and for any system delay. The additional compensation required for

---

* Of course, theoretically, one could simply put lead-lag networks on all display inputs and choose the parameters by "searching" with the OCM.

the system delay is undesirable. The basic idea behind the OCM frequency domain compensator is to relieve the pilot of the necessity for generating the additional lead by approximating the incremental predictive response by the delay compensator. This is accomplished by computing pilot describing functions with and without system delay, calculating the "difference" between these two describing functions, and designing a filter to approximate that difference.

To be more precise, refer again to Figure 4.1 and consider the single-loop case. We assume that the describing function for the full delay condition, H_d, can be factored as

$$H_d(j\omega) \simeq H(j\omega)P_d(j\omega) \qquad (4.10)$$

where P_d is the portion of the delay-modified describing function that compensates for the system delay. Reference to Eq. (2.10) shows that the factorization cannot be done analytically and that only an approximate factorization is possible. If H_d and H are computed, then P_d can be determined easily, at any frequency ω_i, from

$$\text{Magnitude: } \log |P_d(\omega_i| = \log|H_d(\omega_i)| - \log]H(\omega_i| \qquad (4.11)$$

$$\text{Phase: } \measuredangle P_d(\omega_i) = \measuredangle H_d(\omega_i) - \measuredangle H(\omega_i)$$

The delay compensator is then "designed" by finding a rational transfer function to approximate $P_d(j\omega_i)$ for values of ω_i that lie within the man-machine bandwidth. To repeat, the theory is that if the system contains the required compensation, $F \approx P_{\tau_d}$, the pilot should not have to add his own compensation and, therefore, should be able to employ the no-delay strategy.

This method of design has considerable appeal in that it is closed-loop in nature and attempts to restore the pilot's strategy directly. However, it, too, has difficulties in the multivariable case. The basic problem is in deciding which describing functions to use in compensating a given display output. For example, suppose there are two controls and three displayed outputs. Then, there are six equations corresponding to Eq. (4.10), namely

$$H_{d_{ij}}(j\omega) = H_{ij}(j\omega) P_{ij}(j\omega); \; i=1,2; j=1,2,3 \qquad (4.12)$$

The question is how the two predictors, P_{1j} and P_{2j}, should be used to compensate display j. There may be ways to make this choice rationally but we did not pursue the issue further here. Instead, we evaluated the approach for a single-loop problem and went to a more direct method for calculating predictive compensation that also uses the OCM, but in a different fashion. This method is discussed next.

4.4 OCM Time-Domain Compensator

In the previous two sections, delay compensators were derived via frequency domain techniques. The compensators were specified either by classical design criteria, or by an approximate factorization of the pilot describing function predicted by the OCM for the delay condition. A critical shortcoming of these methods is the difficulty in extending them to multi-input, multi-output (MIMO) cases.

Motivated by this shortcoming of the compensators designed by frequency domain methods, a state-space compensator was developed. The basic idea behind the design of this compensator is to use the OCM to develop an analytic expression that can be used directly as a fixed lead predictor for the closed-loop pilot/vehicle dynamics. The use of state-space methods in the design should assure that MIMO problems can be handled easily. To design such a predictor precisely would require including the full OCM in the compensator. This does not appear to be practical so a simplified and straightforward approximate OCM pilot model is used. The remainder of this section will be devoted to a derivation of this simplified compensator.

An equation describing the pilot/vehicle closed-loop system can be obtained using the expressions for the OCM obtained in Chapter 2. If the estimation error is written as

$$\tilde{\underline{x}}(t) = \underline{x}(t) - \hat{\underline{x}}(t)$$

and substituted into equation (2.13), the following expression for the closed-loop dynamics results:

$$\frac{d}{dt}\begin{bmatrix}\underline{x}(t)\\ \underline{u}(t)\end{bmatrix} = \bar{\underline{A}}\begin{bmatrix}\underline{x}(t)\\ \underline{u}(t)\end{bmatrix} + \begin{bmatrix}0\\ \underline{T}_N^{-1}\end{bmatrix}\underline{L}^*\,\tilde{\underline{x}}(t) + \bar{\underline{E}}\begin{bmatrix}\underline{w}(t)\\ \underline{v}(t)\end{bmatrix} \qquad (4.13)$$

where

$$\bar{\underline{A}} = \begin{bmatrix}\underline{A} & \underline{B}\\ \underline{T}_N^{-1}\underline{L}^* & -\underline{T}_N^{-1}\end{bmatrix} \quad ; \quad \bar{\underline{E}} = \begin{bmatrix}\underline{E} & 0\\ 0 & \underline{T}_N^{-1}\end{bmatrix}$$

Equation (4.13) shows the effect of the fixed optimal control gains on the closed-loop dynamics, and intentionally lumps the frequency dependent Kalman filter/predictor effects into $\tilde{\underline{x}}(t)$.* To include these effects explicitly would require maintaining Kalman filter state estimates in this closed-loop description, thereby doubling the order of the system of equations considered.

Given Eq. (4.13) and assuming $\tilde{\underline{x}}(t)$ is a white, zero mean, gaussian random process, and that $\underline{x}(t)$, $\underline{u}(t)$ are available in the simulation, the optimal linear fixed-lead predictor can be written as: (see Sage and Melsa (1971) for a complete derivation)

---

* The control gains, $\underline{L}^*$, are not the same as pilot gain as measured by the describing function amplitude. Pilot gain is a function of all portions of the OCM.

$$\begin{bmatrix} \underline{x}_p(t+\tau_d) \\ \underline{u}_p(t+\tau_d) \end{bmatrix} = \Phi(\tau_d) \begin{bmatrix} \underline{x}(t) \\ \underline{u}(t) \end{bmatrix} \tag{4.14}$$

with $\Phi(\tau_d) = e^{\bar{A}\tau_d}$ and where τ_d is the display delay to be compensated for. Notice that this form is the same as would have been obtained for the noise-free case. Further, the same predictor is obtained by simply ignoring the Kalman filter/predictor structure in the formulation of the pilot model. Although Eq. (4.14) represents the best linear predictor in the mean-squared error sense, the predicted estimates can exhibit large variances (Sage and Melsa (1971)). Therefore, one may expect the predictor to be most useful for "small" values of τ_d, unless the process noise (including pilot remnant) is very small.*

Assuming τ_d is of reasonable magnitude, equation (4.14) defines a candidate compensator structure. Although the compensator is the best linear predictor, there is no guarantee that its inclusion will produce the desired "no-delay" performance or pilot strategy -- especially since the OCM's (and, presumably, the pilot's) filtering and prediction were ignored in predicting closed-loop behavior. Indeed, it turned out in a preliminary evaluation of the compensator that direct use of Eq. (4.14) did not

* Noise filters could be cascaded with this compensator to increase the range of delays which can be considered.

yield the desired results. In particular, the low frequency gain of the predicted describing function with compensation was too low and the tracking error too large.

The failure of the compensator to restore performance in preliminary tests suggested that ignoring the Kalman filter completely in deriving the predictor was too simple an approximation. For a fixed process noise, the Kalman filter gains are determined largely by the observation noise levels. Thus, one possible way to account for these gains is to adjust the observation noises with compensation to match those of the no-delay case. Because, in the OCM, the observation noises are multiplicative in nature, this can be accomplished by adding to the compensator a noise equalization scale factor, K_i, for each display signal. Note, that for implementation reasons, only the signals driving the displays are scaled and not their derivatives which are included in the "display" vector to model the pilot's rate perception capability. Thus, if it is assumed that the display outputs are ordered in position-rate pairs, then only the odd-numbered outputs are scaled in the OCM analysis. The compensation equation for each display is then given by

$$Y_{c_i}(t+\tau_d) = K_i [\underline{C} \quad \underline{D}]_i \, \underline{\Phi}(\tau_d) \qquad ; i=1,3,\ldots m-1 \quad (4.15)$$

where $[\ \cdot\ ]_i$ denotes the ith row of the matrix.

Two further points concerning the time domain compensation should be mentioned. First, for the single input/single output case, if K<1, the effective vehicle gain observed by the pilot will be reduced. This should result in an increase in pilot gain and a reduced mean-squared observed error, which are the desired efforts. Second, the form of compensation indicated by Eq. (4.15) is simply a linear combination of state and control variables. In general, this implies derivative information being used in the compensator so that lead is provided. Normally, this form of compensation affects only the zeros of the closed-loop system. However, adjusting the noise levels with the equalization factor, will result in a slight shift of the closed-loop poles. Nonetheless, it may be necessary, in actual implementation of the compensator, to include some noise filtering.

Figure 4.3 shows the compensator as it would appear in an actual simulation. Note that the matrix $\underline{K}$ is diagonal with elements K_i. In modelling this situation via the OCM, however, one must provide the derivative of the display variable to the human operator. Thus, the derivative of the predicted y is needed, and not the <u>prediction</u> of $\dot{y}$ which could be obtained directly from Eq. (4.14). Differentiation of equation (4.15) yields:

$$\frac{\partial}{\partial t}\underline{y}_c(t+\tau_d) = K[C\ D]\quad \Phi(\tau_d)\quad \begin{bmatrix}\dot{x}\\ \dot{u}\end{bmatrix} \tag{4.16}$$

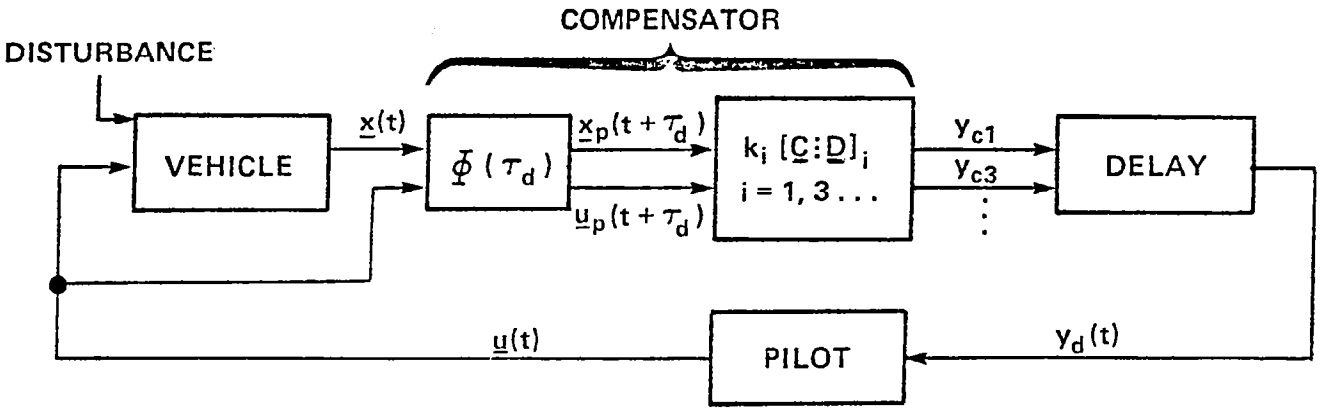

Figure 4.3. OCM Time Domain Compensator

Notice $\dot{\underline{x}}(t)$ is available from the model of the plant but $\dot{\underline{u}}(t)$ is not available. To circumvent this problem, the following "trick" is emp_oyed in the OCM analysis. A lowpass filter of the form

$$\frac{y_{OUT}}{y_{IN}} = \frac{p}{s+p} \tag{4.17}$$

is introduced in series with each display signal. The pole of the filter, p, is chosen large enough to insure that minimal gain and phase distortion occurs in the bandwidth of interest. In particular, p=60 rad/s was the value chosen for the subsequent analyses. Note that for frequencies well below p, $y_{IN} = y_{OUT}$. If the corresponding state equation for the filter is written, it provides an expression for $\dot{y}(t+\tau_d)$ which <u>does not</u> involve $\dot{u}$. Specifically,

$$\dot{y}_{OUT} = pY_{IN} - pY_{OUT} \qquad (4.18)$$

In summary, the OCM time domain compensator will be determined via a model analysis involving the following steps:

1. Run the OCM with no display delay saving $\underline{L}^*$ and $\underline{T}_N^{-1}$ and note measurement noise levels ($\underline{V}_y^{ND}$).

2. Form $\underline{\Phi}(\tau_d)$ using $\underline{L}^*$ and $\underline{T}_N^{-1}$ computed in step 1.

3. Set $\underline{K} = \underline{I}$.

4. Augment plant state equations to include lowpass filters (for output rate reconstruction).

5. Run the OCM (with the compensator present) - note measurement noise levels ($\underline{V}_y^c$).

6. Compare $\underline{V}_y^c$ with $\underline{V}_y^{ND}$

   - if close enough, go to step 8

   - else, go to step 7

7. Pick a new $\underline{K}$ by an appropriate search scheme; go to step 4.

8. Finished -- use current compensator structure.

5. COMPENSATOR RESULTS

In the previous chapter, three delay compensators were proposed and developed. In this chapter, each compensator is evaluated on the basis of its ability to reproduce no-delay performance in a simple roll-axis tracking task. Based on these results, the most promising compensator is selected for later use in the multi-axis RSRA problem. This compensator is then tested, in the roll tracking task context, for robustness to changes in pilot parameters. Finally, the chosen compensator is applied to the RSRA hover task.

5.1 A Roll Tracking Task

The initial design and evaluation of the delay compensation schemes in the full RSRA task is difficult because of the complexity of the task. Therefore, it was decided to first study the compensators in a simpler, more easily interpreted context. The task chosen for this preliminary evaluation was a roll tracking task that was similar to that used by Crane (1980).

The roll tracking task is illustrated in Figure 5.1. The vehicle transfer function was assumed to be

$$\frac{\phi}{u} = \frac{6.25}{s(s+6.25)} \tag{5.1}$$

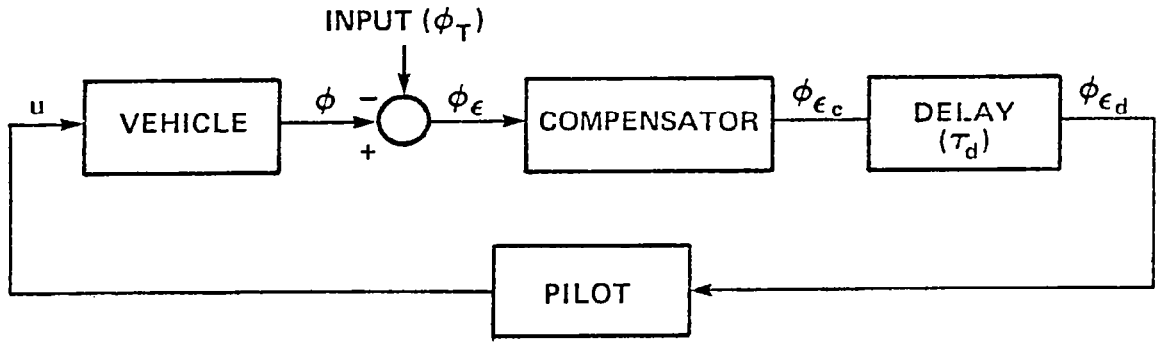

Figure 5.1. Block Diagram for Roll Tracking Task

Target motion was assumed to be generated by passing white noise through a filter approximating the vehicle transfer function, that is, by

$$\frac{\phi_T}{w} = \frac{1}{(s+1)(s+6.25)} \tag{5.2}$$

The pole at .1 rad/s is included to avoid the anomaly of integrating white noise, which gives infinite variance. Vehicle dynamics are a low-order approximation to those used by Crane (1980). The input was chosen to yield a display change that approximates the vehicle's response to a wide-band disturbance; this is in the spirit of the manner in which the input was chosen for Crane's study. The state equations for this problem are given in Table 5.1.

Table 5.1. Roll Tracking Task Dynamics

STATE EQUATIONS FOR ROLL TRACKING TASK
STATES:PHI-TARG-DOT,PHI-TARG,PHI-VEH.-DOT,PHI-VEH.
OUTPUTS:ROLL ERROR,ROLL ERROR-RATE

A MATRIX:

-6.350E+00	-6.250E-01	0.	0.
1.000E+00	0.	0.	0.
0.	0.	-6.250E+00	0.
0.	0.	1.000E+00	0.

B MATRIX:

0.
0.
6.250E+01
0.

E MATRIX:

1.000E+00
0.
0.
0.

C MATRIX:

0.	-1.000E+00	0.	1.000E+00
-1.000E+00	0.	1.000E+00	0.

D MATRIX:

0.
0.

The roll tracking task was analyzed with the OCM, using standard parameters for the pilot model, as listed in Table 5.2.

A computational delay of .Ø18 seconds was assumed and display delay was varied from Ø-.Ø96 seconds to correspond to the experimental situation described in Crane (198Ø). Mean-squared errors and pilot and open-loop describing functions were computed as a function of delay with the OCM. The results are shown in Figures 5.2 and 5.3 and later in 5.5.

Figure 5.2 compares computed and experimental effects of delay on performance scores. The experimental scores are the average of five pilots, each flying eight trials at each condition (Crane (198Ø)). Both the experimental and computed scores are normalized by their respective zero-delay values so that a comparison of the relative effect of delay may be made. As can be seen, model results predict the effect of delay on tracking error quite well. Though not shown, it should be noted that the model-data differences that exist are well within the range of subject-to-subject variability.

The effects of delay on selected frequency domain parameters are shown in Figure 5.3.* Specifically, closed-loop system

* Complete pilot describing functions and open-loop describing functions predicted by the OCM will be presented later.

Table 5.2 Nominal OCM Parameter Values for Roll Tracking Task

OCM PARAMETER	VALUE
Pilot Delay, τ_H	.2 sec
Neuro Motor Time Constant, T_N	.1 sec
Observation Noise/Signal Ratio, P_y	-20 dB
Motor Noise/Signal Ratio, P_m	-25 dB

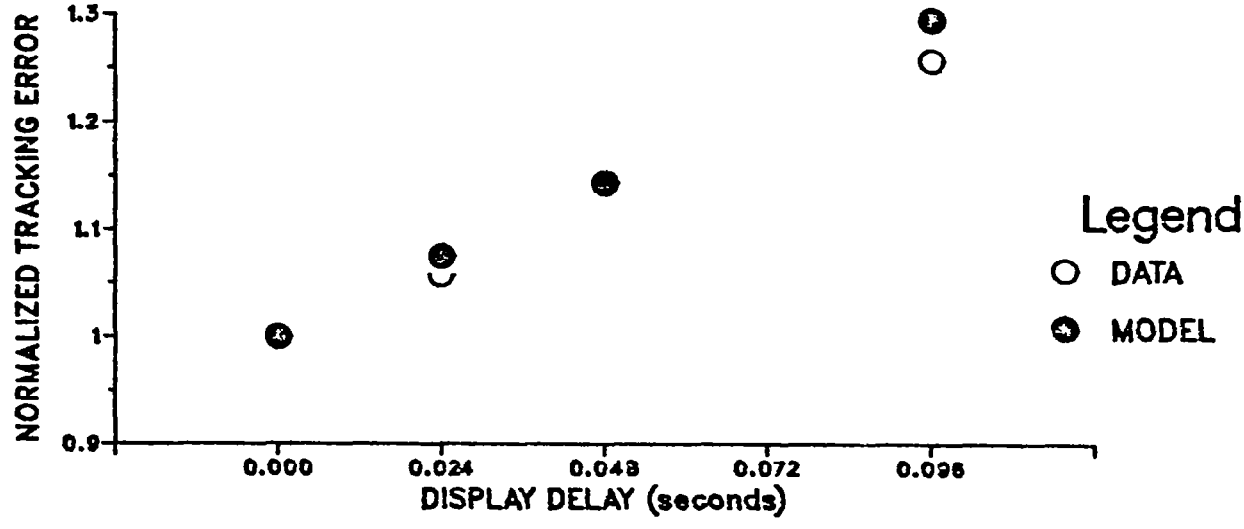

FIGURE 5.2 EFFECT OF DELAY ON ROLL TRACKING ERROR

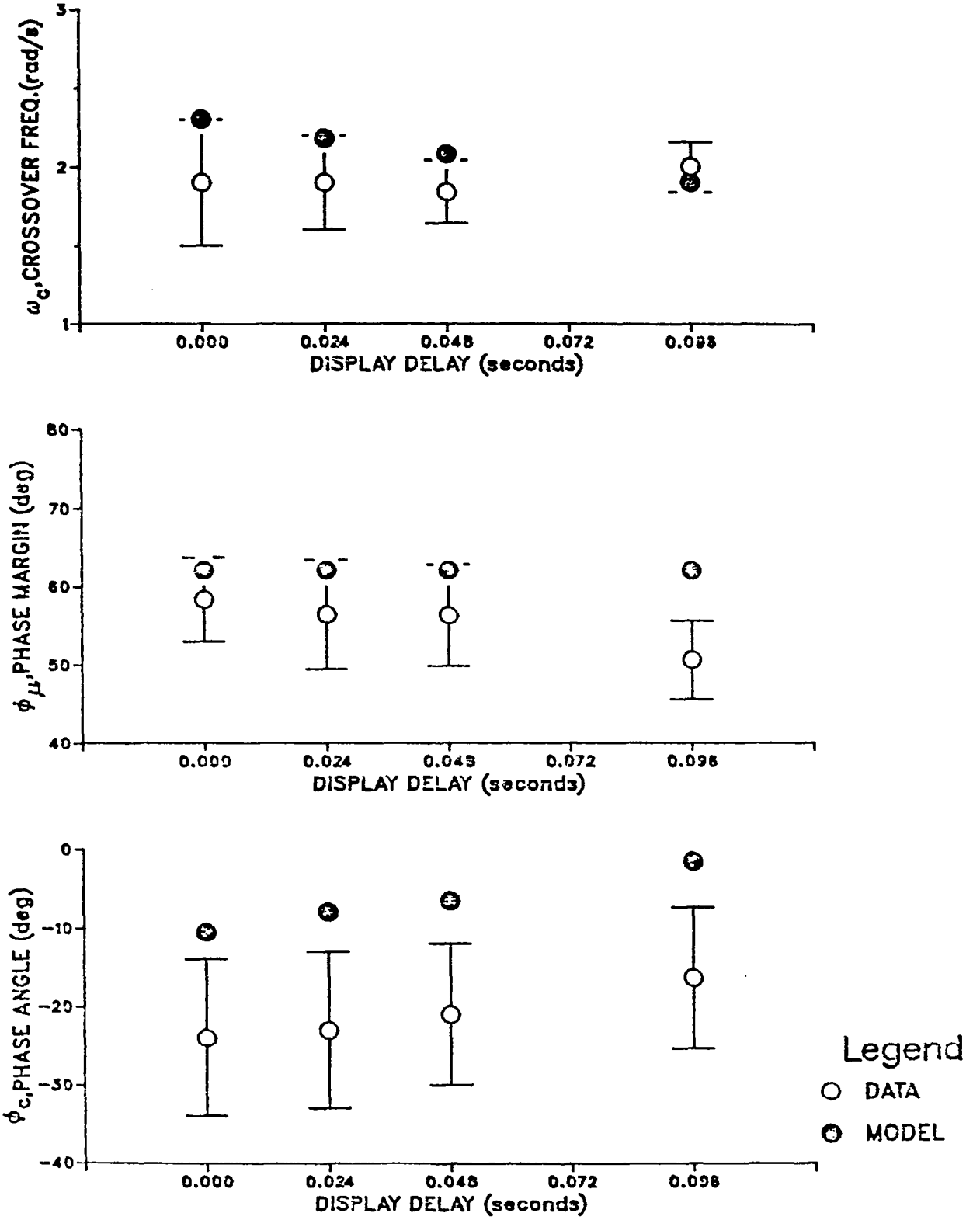

FIGURE 5.3 EFFECT OF DELAY ON FREQUENCY DOMAIN MEASURES (ROLL–TRACKING TASK)

crossover frequency ω_c and phase margin ϕ_m and the phase angle of the pilot's describing function at ω=3.27 rad/sec, ϕ_p, are plotted as a function of delay. The experimental measures are the values averaged across trials and subjects. Also shown are the across-subject standard deviations of the measures. Note that ω_c and ϕ_m are estimated by interpolation, for both data and model.

The data do not reflect a clear trend in system crossover frequency with delay. Moreover, the detailed statistical analysis reported in Crane (1980) reveals a statistically significant pilot variation. On the other hand, the average phase margin appears to be decreasing with delay and the decrease is reported to be statistically significant. Pilot phase angle at 3.27 rad/sec, that is, slightly beyond crossover, shows that as delay was increased, the pilots decreased their phase lag (added lead) and the effect was significant. This, as noted elsewhere, is consistent with expectations concerning increased workload resulting from delay.

The model results for the frequency domain measures are comparable in magnitude to the data, though there appear to be some differences in the trends exhibited by the system parameters. Thus, the OCM reduces crossover frequency (i.e., lowers pilot gain) with increasing delay while maintaining the phase margin virtually constant, whereas the data show no clear trend for crossover frequency and some reduction in phase margin with increasing delay.

Model predictions are, for the most part, within one standard deviation of the mean for these system measures at all values of delay considered, so it is difficult to evaluate the importance of these differences in trend. In addition, there has been no "tuning" of model parameters to bring the results in closer agreement. Thus, a small change in assumed pilot delay and/or T_N could produce even better agreement.

The OCM predicts a reduction in pilot phase lag that is very nearly the same as that measured experimentally. The differences in absolute value of pilot phase are readily accounted for by assuming a slightly higher base value for the nominal pilot delay. Thus, an increase of the nominal delay to .25 seconds, which is not an unusual value for the human's delay, will subtract ten degrees from the model delay shown and will bring the OCM results and the data for phase lag in virtual correspondence.

In summary, the OCM predicts accurately the changes in performance and pilot lead with increases in display delay that are measured in a comparable, single-axis experimental task. The results with respect to system crossover frequency and phase margin are more difficult to interpret. The OCM appears to respond to increases in delay by reducing low frequency gain (and thereby crossover frequency) so as to maintain a fixed phase margin, if possible. The data suggest that, on average, the pilots may be

attempting to keep crossover fixed while yielding some phase margin in the process.

5.2 Compensators for Roll Tracking Task

Compensators were designed for the above task by the three methods described in Chapter 4. The specific parameters used in the design are delineated in this section.

5.2.1 Classical Compensator

A family of classical lead-lag compensators was designed using Eq. (4.9), with T_1 as a parameter of the design. The nominal value of T_1 was determined from the OCM analysis of the roll tracking task which yielded T_1=.4 seconds (ω_c~2.3 rad/sec) for the no-delay case. Table 5.3 shows the ratio of compensated performance to no-delay performance for various values of T_1, where performance is the mean-squared tracking error observed by the pilot.

Table 5.3 Effect of Lead Time Constant on Performance of the Classical Compensator

T_1 (seconds)	$\frac{\overline{\phi_{\varepsilon_c}^2}\ \text{(compensated)}}{\phi_{\varepsilon}^2\ \text{(NO-DELAY)}}$
0 (NO COMPENSATION)	1.30
.555	1.38
.400	1.29
.333	1.22
.222	.99

Based on the results given in Table 5.3, the following lead-lag compensator was chosen for further analysis:

$$\frac{\phi_{\varepsilon_c}}{\phi_\varepsilon} = .753 \left(\frac{.222s+1}{.082s+1}\right) \triangleq F_c(s) \tag{5.3}$$

The frequency response of F_c is shown below in Figure 5.4.

5.2.2 OCM Frequency Domain Compensator

To design the OCM frequency domain compensator, the predicted pilot describing functions for the no-delay and .Ø96 second delay (with no compensator) were computed. The added prediction necessitated by the delay was then estimated using Eq. (4.11) with the result shown as P_d in Figure 5.4. This computed frequency response was then "fit" by a rational transfer function that had a first order polynomial in the numerator and a second order polynomial in the denominator. The fit was chosen to provide the closest approximation in the neighborhood of the predicted crossover frequency. The transfer function of the resulting compensator, also shown in Figure 5.4, is given by

$$F_{OCMF}(s) = \frac{172.5(.132s+1)}{(s^2+15.9s+227)} \tag{5.4}$$

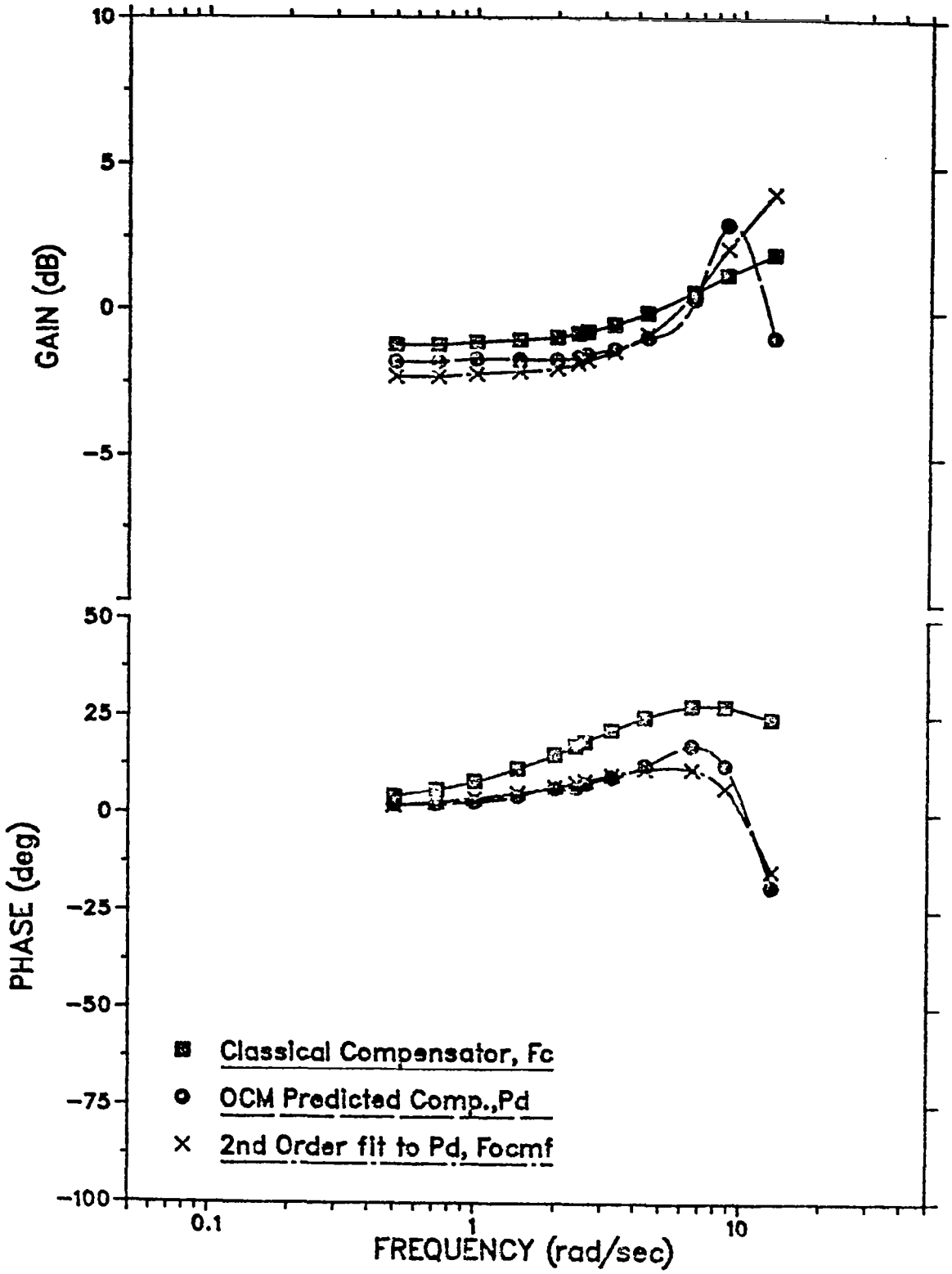

FIGURE 5.4: Frequency Responses of Classical and OCM Frequency Domain Compensators

Reference to Figure 5.4 shows that, in the range $1<\omega<13$, the OCM-based compensator provides from about five to twelve degrees less lead than does the classical compensator and has a slightly lower gain.

5.2.3 OCM Time Domain Compensator

The OCM time domain compensator is designed by computing the control gains for the problem (which are independent of the delay) and then determining the factor K (which is a scalar constant in this case) by an iterative model analysis. For the roll tracking task, the gains and scale factor are

$$L^*=[-0.841 \; -6.64 \; 0.857 \; 6.74]$$

$$T_N^{-1}=10.35$$

$$K=.92$$

5.3 Analysis of Compensator Performance

As mentioned earlier in this report, one can view the goal of the compensation scheme in various ways. For example, one can introduce compensation in an effort to duplicate the pilot strategy adopted for the no-delay case, or to best match the open-loop vehicle/compensator dynamics. In the following discussion, the three compensator designs will be compared from several viewpoints.

Figure 5.5 shows the effect each compensation scheme has on the pilot describing functions predicted by the model. The pilot describing function is defined as the transfer function from y to u through the OCM pilot model, and as such, defines the adopted pilot "strategy" for the various configurations. The phase portion of Figure 5.5 shows that with no compensation, but full display delay (bullet), the pilot must introduce (a maximum of) approximately 20^{o} more phase lead at ω=7 rad/s than for the no-delay case (box). All of the compensators reduce the requirements for added pilot phase lead. However, both of the OCM-based compensators appear to provide a better match to the desired no-delay phase than the classical compensator. The corresponding gain curves show that, at frequencies up to about 4 rad/sec, all compensators yield a predicted pilot gain that lies between that for the no-delay and full-delay cases. Moreover, all the gain differences in this region are relatively small (<2.5 dB). Larger discrepancies are apparent in all compensated cases at the higher frequencies, where the effects on performance of gain mismatch are less important. Over the entire frequency range of interest, the OCM time domain compensator (ring) provides the closest match to the no-delay pilot gain, even doing the best job of mimicking the resonance characteristic in the region around ω=10 rad/sec.

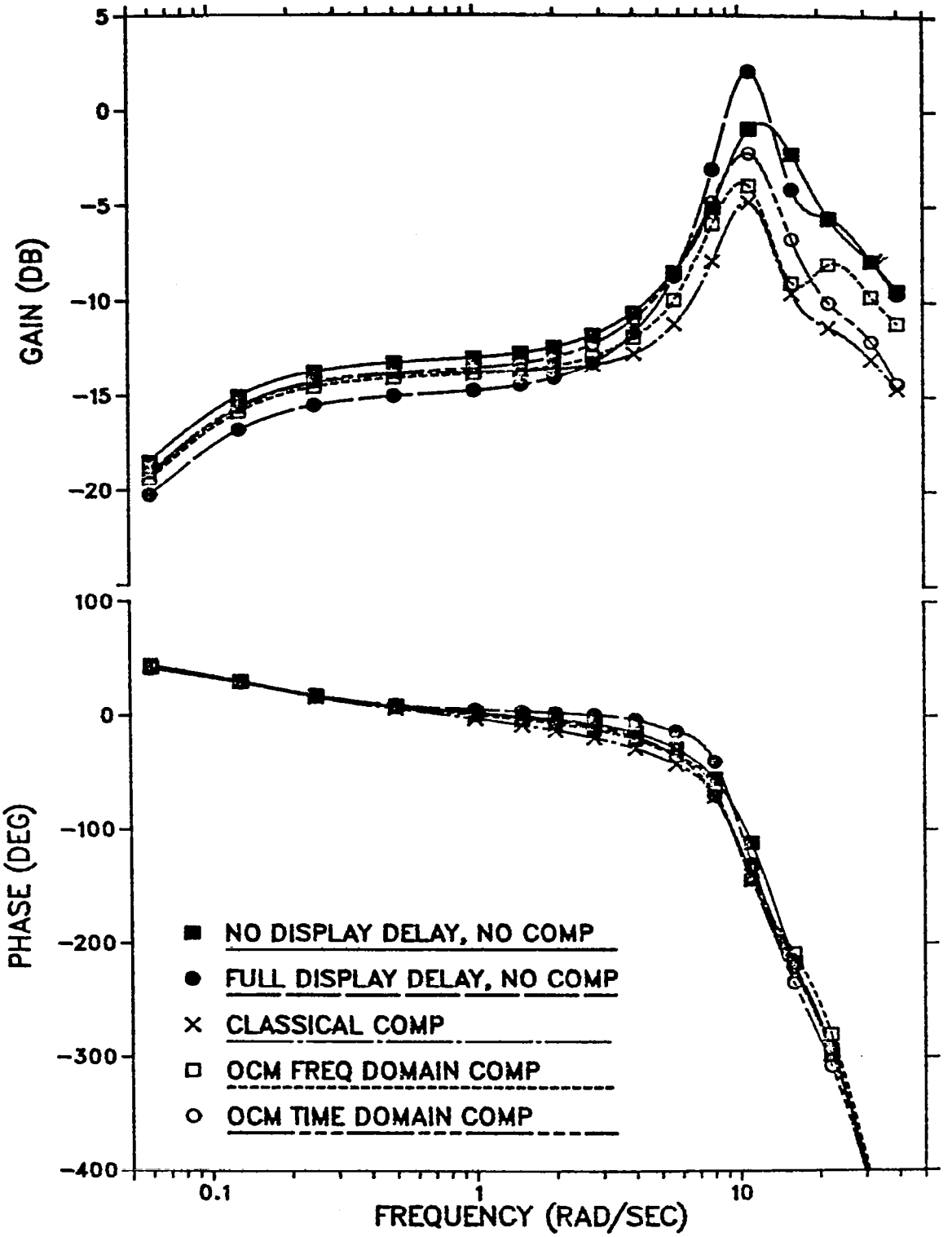

FIGURE 5.5: EFFECT OF COMPENSATION ON PILOT DESCRIBING FUNCTION (ROLL TRACKING TASK)

The effects of compensation on "perceived" open-loop vehicle transfer function are seen in Figure 5.6. This transfer function is defined as the transfer function between the pilot control input and the displayed output and, of course, includes any delay compensator and/or display delay which may be present. To obtain a "feel" for this transfer function, notice that the no-delay (box) and full-delay (bullet) gain curves are identical, while the full-delay phase rolls off at a faster rate. This should be intuitive since the transfer function, for a pure delay element, is characterized by unity gain and a phase lag that increases proportionally with frequency.

The ideal compensator strives to match the no-delay phase curve with minimum gain distortion. The high frequency phase differences are dramatic, with the OCM time domain compensator out-performing the others. However, the classical compensator (cross) shows the best match for frequencies between 1 and 8 rad/s. The gain portion of Figure 5.6 shows that the OCM time domain compensator best matches the no-delay gain over the largest frequency band. This compensator results in approximately a constant 1 dB error in gain, while both other compensators yield a constant 2 dB error. Notice the high frequency gain distortion for the OCM time domain compensator. The shape is typical of lead generated by moving only the zeros of the open-loop dynamics. The

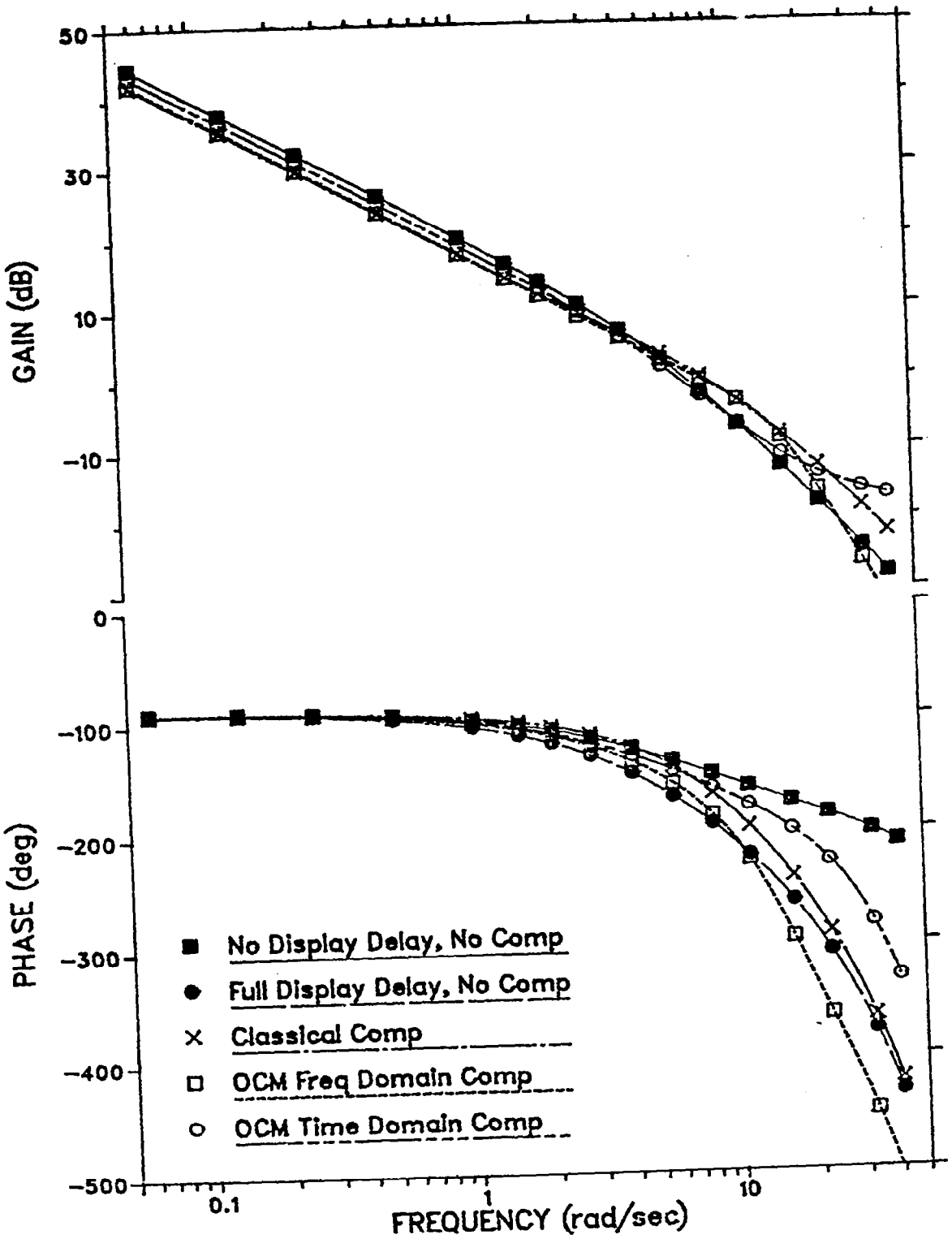

FIGURE 5.6: Effect of Compensation on Perceived Vehicle Transfer Function (Roll Tracking Task)

implications of this gain distortion are that it will allow more (high frequency) process noise to enter into the display. In this case the distortion is small and below unity gain; however, it does show a potential problem with this type of compensation (one which could be lessened with an appropriately selected noise filter).

Figure 5.7 shows the effect of the compensators on the open-loop pilot/vehicle describing function. For single loop problems, such as the roll tracking task, this corresponds to the $Y_p Y_c$ transfer function referred to earlier. The principle use of this describing function is to determine the gain and phase margin of a given loop closure.

The gain and phase margins for the various cases were determined graphically. The gain margins are all approximately 7.5 dB. The phase margins for the no-delay, full-delay and OCM time domain compensator cases are all about 61 degrees whereas the classical and OCM frequency domain compensators produce slightly greater phase margins ($\approx$66.5) degrees. In general, these differences are not likely to be very significant.

The ability of a compensator to generate a match to various performance levels found in the no-delay situation is another important indication of the compensator's effectiveness. Table 5.4 displays the rms scores predicted by the OCM for each condition.

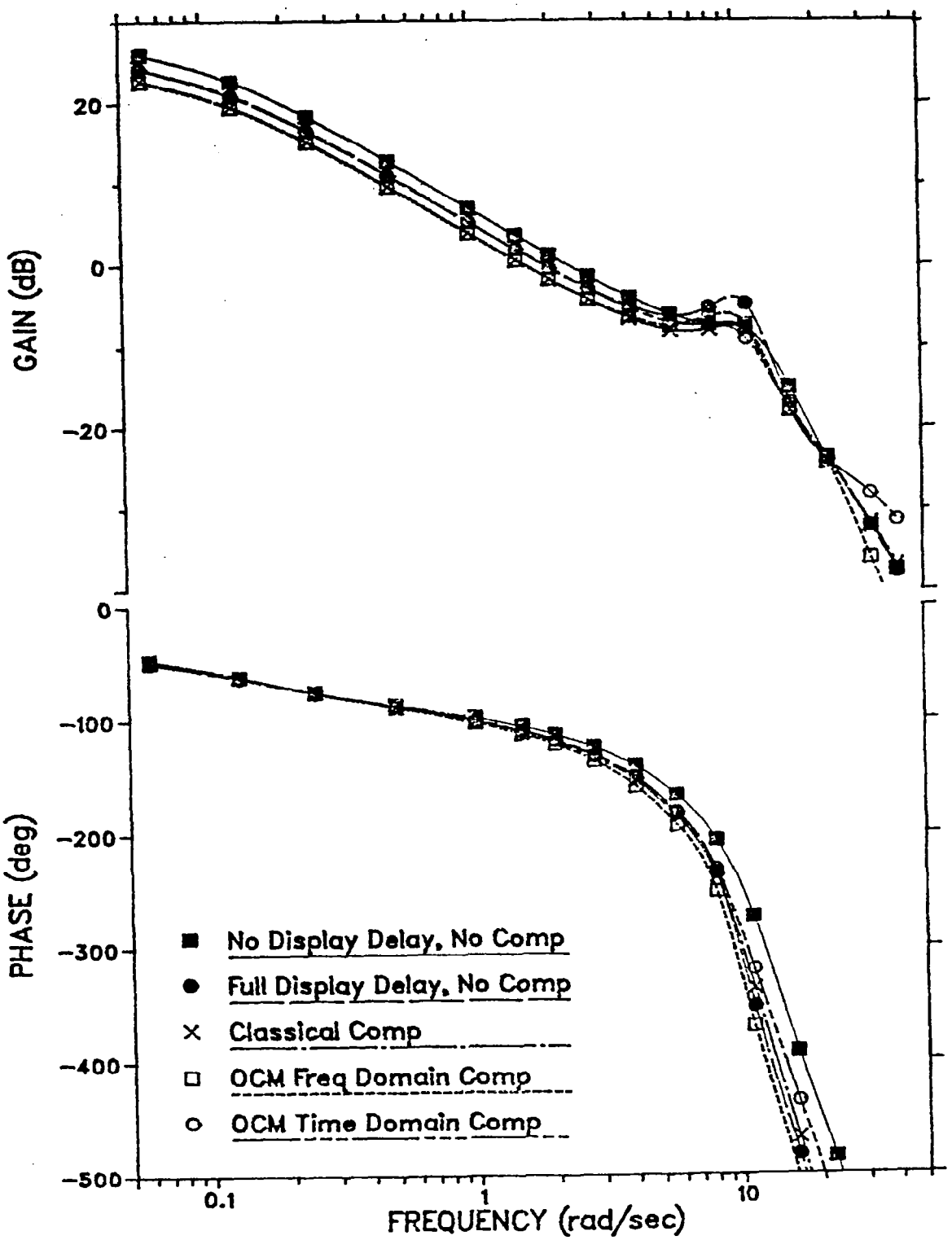

FIGURE 5.7: Effect of Compensation on Open-Loop Describing Function (Roll Tracking Task)

Included in the table are scores for roll error ϕ_e, roll rate error $\dot{\phi}_e$, pilot control u, and control rate $\dot{u}$. In addition, the last column contains computed values for the cost functional J. As mentioned in section 2.3.2, J is a measure of pilot performance which can be related to workload if one considers that, in order to maintain a desired performance level, pilot attention to the task must vary. With this in mind, Table 5.4 shows a 25% decrease in performance when the display delay is present, but no compensation is used (as noted in Figure 5.2). Inclusion of any of the compensators, as designed, results in a restoration of performance back to no-display delay levels (with a corresponding decrease in pilot workload). Since, in this task, J is a weighted sum of only roll error variance and control-rate variance, lowering J is tantamount to matching roll error and control-rate variances. From the table we see that, whereas all compensators can match roll error equally well, the OCM time domain compensator does significantly better in matching control scores.

Table 5.4. Computed RMS Error Scores vs. Condition - Single Axis

Condition \ Variable	ϕ_{ε_c}	ϕ_{ε_c}	u	$\dot{u}$	J
No Delay, No Comp	3.82	15.0	1.29	9.84	16.8
Full Delay, No Comp	4.34	15.2	1.29	9.88	21.0
Classical Compensator	3.82	17.9	1.02	7.36	15.8
OCM Frequency Domain Comp.	3.81	14.5	1.06	7.45	15.7
OCM Time Domain Comp.	3.82	18.7	1.21	8.82	16.3

In terms of the other scores shown in Table 5.4, we see that with no compensation present, both roll-rate error and control scores are insensitive to display delay variations. However, introduction of the compensators causes a scaling of these scores. Control scores are 21% lower than desired with both the classical and OCM frequency domain compensators, while only 6.2% lower for the OCM time domain compensator. The OCM frequency domain compensator results in a good match to roll-rate error. Roll-rate error is not matched as well by the other two compensators, with a 20% and 24.6% matching error for the classical and OCM time domain compensators, respectively. In the case of the OCM time domain compensator, this mismatch may be due to the approximate way in which the error-rate signal was modelled.

Based on the single-axis results presented above, the OCM time domain compensator was selected as the compensation scheme best able to replicate the desired no-display delay conditions. This, however, is not to say that the other methods are without merit. On the contrary, in many instances, they performed just as well as the selected scheme. However, the ability of the OCM time domain compensator to be extended relatively easily to the MIMO case is certainly desirable, inasmuch as we wish to compensate the RSRA problem discussed in Chapter 3. In the next section, the robustness of the selected compensation scheme to unaccounted-for pilot differences will be examined.

5.4 Investigation of Robustness of OCM Time Domain Compensator to Pilot Variations

As recalled from section 4.4, the OCM time domain compensator is based on nominal OCM pilot parameters and, therefore, is "tuned" to an "average" pilot.* In reality, individual pilots may differ significantly from this "average" pilot model; i.e., the parameters of the OCM characterizing an individual's response may differ from the nominal parameters used in the design. Therefore, it is important to examine the sensitivity of the pilot/vehicle-compensator closed-loop system to expected inter-pilot variations. In this section, the OCM will be used to simulate individual pilot differences by varying selected OCM parameter values. The OCM time domain compensator, with parameters unmodified from those defined in the previous section for the roll tracking task, will be used for delay compensation in the remainder of this section. Performance will be observed for each characteristic change in pilot model parameters under no-display delay, full display delay and compensated conditions. Notice the comparison corresponds to a situation in which the same individual performed the task under all conditions.

---

* The other compensation methods are tuned in a similar fashion.

From an ongoing study in which the OCM was used to match individual pilot responses obtained from experimental data, specific model parameters were identified as being particularly sensitive to inter-pilot variations. The findings of this study indicate that perturbations in three OCM pilot parameters could account for most of the inter-pilot variations measured. The parameters and their range of variation are as follows: pilot control bandwidth (T_N) $\pm$ 20%, pilot internal delay (τ_H), $\pm$ 15%, and pilot observation noise/signal ratio (P_Y) $\pm$ 3 dB. Inasmuch as these findings represent our best guess at how individual pilots can be modelled using the OCM, they will be adopted for this study. Moreover, the results which follow will be presented as performance variations relative to individual changes in these aforementioned model parameters, rather than to arbitrary mixtures of model parameters representing specific pilots. The basic assumption behind this approach is that performance effects, due to individual model parameter variations, add linearly.

In the figures which follow, the difference between compensated performance and the desired no-delay performance is accented by a shaded area. In interpreting the figures, remember that, in each instance, we are essentially attempting to mimic the performance of an "individual" pilot operating the simulation with no display delay, full display delay, and full display delay plus delay compensation designed for an "average" pilot.

Figure 5.8 shows the sensitivity of roll angle error to variations in T_N. As we saw in the last section, for a nominal value of T_N (.1) the compensator reduces the full delay error (bullet) to the no delay value (approximately a 13% reduction). Since the compensator was "tuned" to this pilot parameter, this is not so surprising. However, for variations of ±20% about the nominal value the compensator still performs quite well. In general, the compensated results differ from the desired results by a larger amount as the pilot bandwidth decreases (increasing T_N). This seems reasonable since, as the pilot becomes more sluggish, errors in prediction (due to use of the wrong closed-loop matrix $\bar{A}$) become more pronounced. Interestingly, the compensated results are linear in T_N, whereas the uncompensated ones are not.

The sensitivity of roll angle error to variations in the pilots internal delay, τ_H, is shown in Figure 5.9. A variation of ±15% about the nominal value of .2 seconds is displayed. In general, we see that roll error is quite insensitive to variations in pilot time delay, with only a 1% variation about the value obtained for a pilot delay equal to that used in the design. For pilots with internal delays smaller than .2 seconds, delay compensation produces slightly larger errors than desired, while smaller errors are predicted for pilots with larger delays.

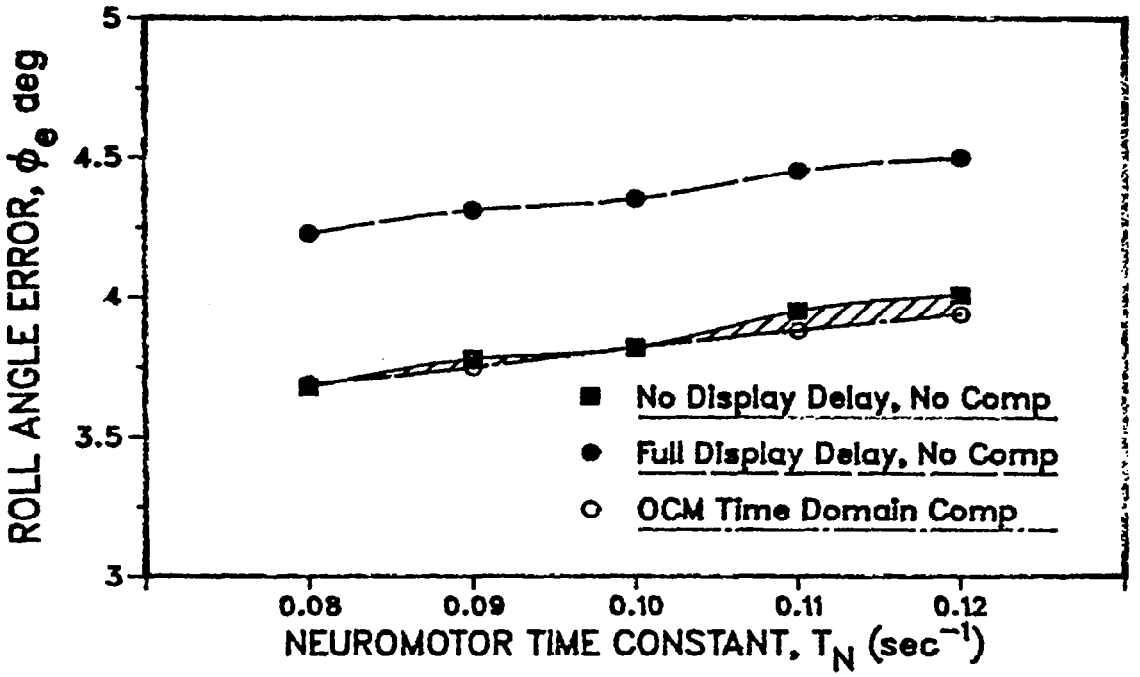

FIGURE 5.8: Sensitivity of Roll Angle Error to Variations in T_N (Roll Tracking Task)

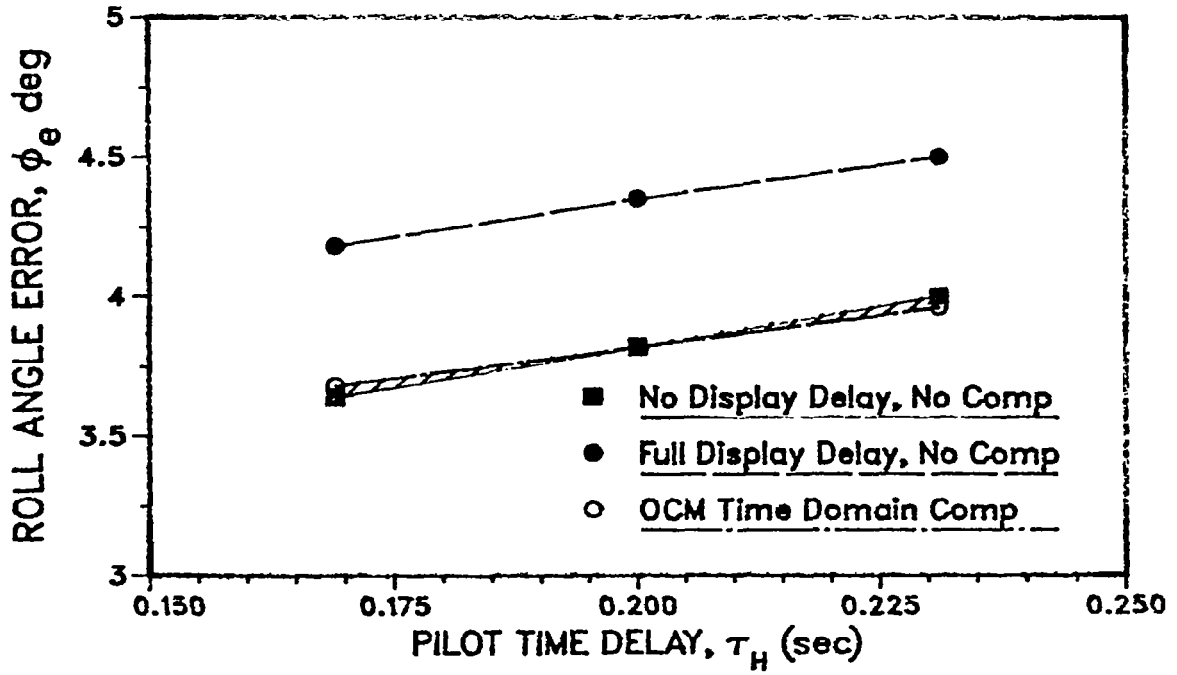

FIGURE 5.9: Sensitivity of Roll Angle Error to Variations in τ_H (Roll Tracking Task)

Figure 5.1Ø shows the sensitivity of roll angle error to variations in pilot observation noise/signal ratio. As stated earlier, one can expect a ±2 or 3 dB variation in observation noise ratio between pilots. Figure 5.1Ø shows a +6 to -3 dB variation

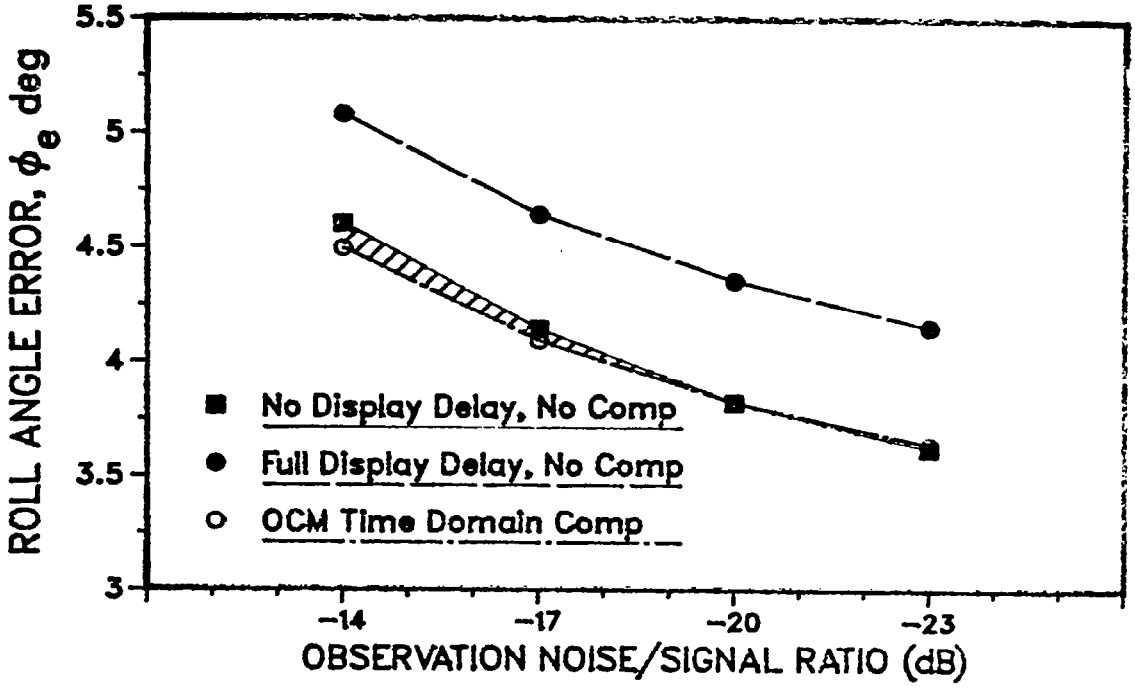

FIGURE 5.10: Sensitivity of Roll Angle Error to Variations in Observation Noise/Signal Ratio (Roll Tracking Task)

about the nominal value of -2Ø dB. Here, as in the previous two plots, we see the characteristic (constant) separation between full-delay and no-delay conditions. The predicted roll error for

the compensated condition matches the desired error quite well, with a value always less than the desired one. Notice that, as the pilot noise increases, so does the compensator mismatch error. This sensitivity is to be expected since increasing the observation noise changes the Kalman filter gains, and the closed-loop dynamics used in the compensator design included a very simple model for the Kalman filter dynamics. Moreover, decreasing the noise (to -23 dB) corresponds better to the assumptions used in the compensator design process, and as a consequence the compensator and no-delay conditions are identical.

The next two figures, 5.11 and 5.12, show the sensitivity of pilot describing function to T_N and T_H variations, respectively. In interpreting these curves, consider that if the compensator was "perfect", (i.e., it could eliminate the display delay effects with no distortion to the describing function), the square would be superimposed on the box and the ring would be superimposed on the bullet. The shaded areas on the curves accent deviations from this case. A comparison of figures 5.11 and 5.5, shows that the differences due to T_N variations are of the same order of magnitude as those found for the nominal conditions, with slightly higher matching error for the quicker pilot (T_N=.08) and lower error for the more sluggish pilot (T_N=.12). For example, looking at the low frequency gain differences, we see that for T_N=.08, there is

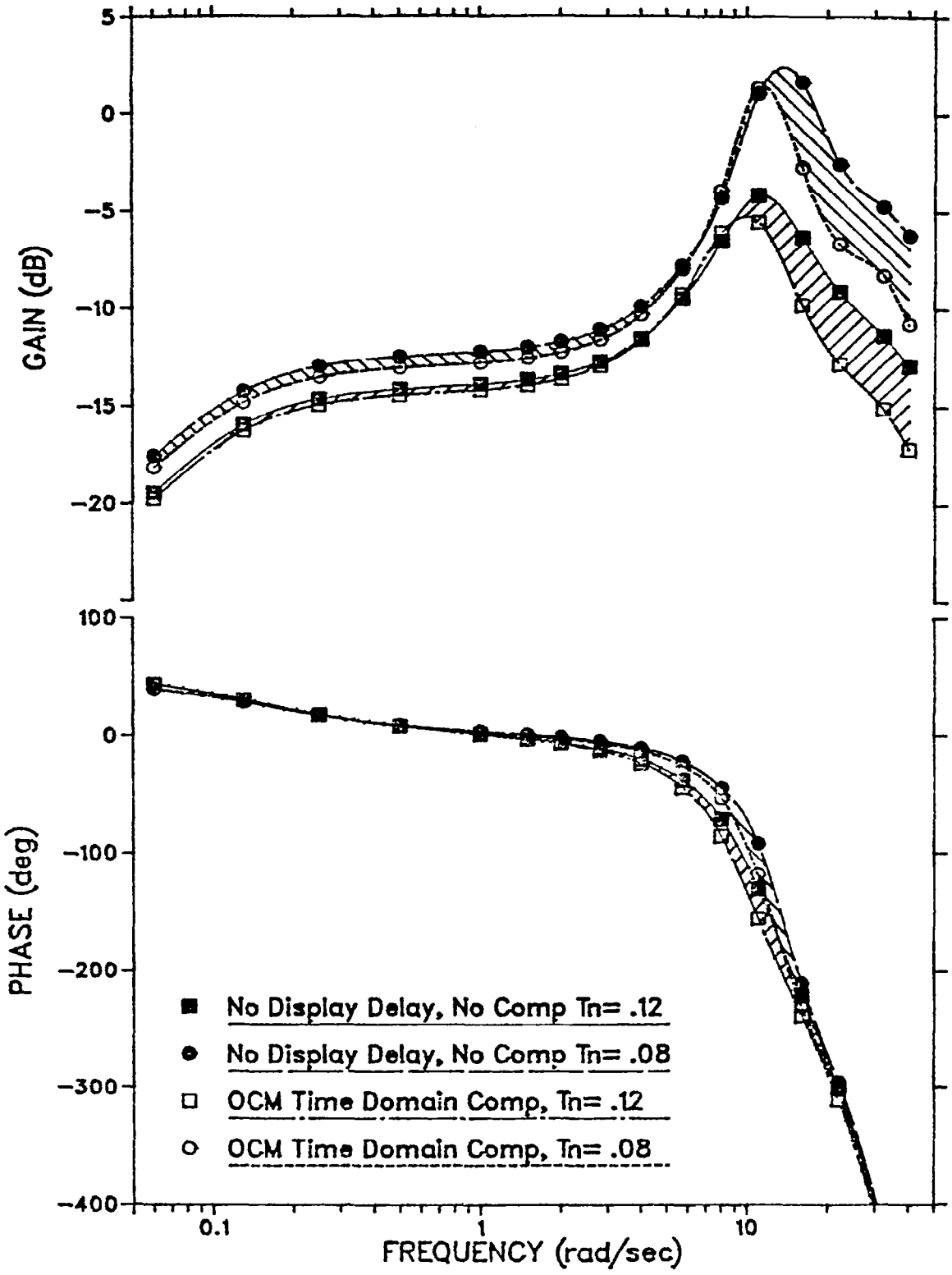

FIGURE 5.11: Sensitivity of OCM Time Domain Compensator to T_N Variations — Pilot Describing Function

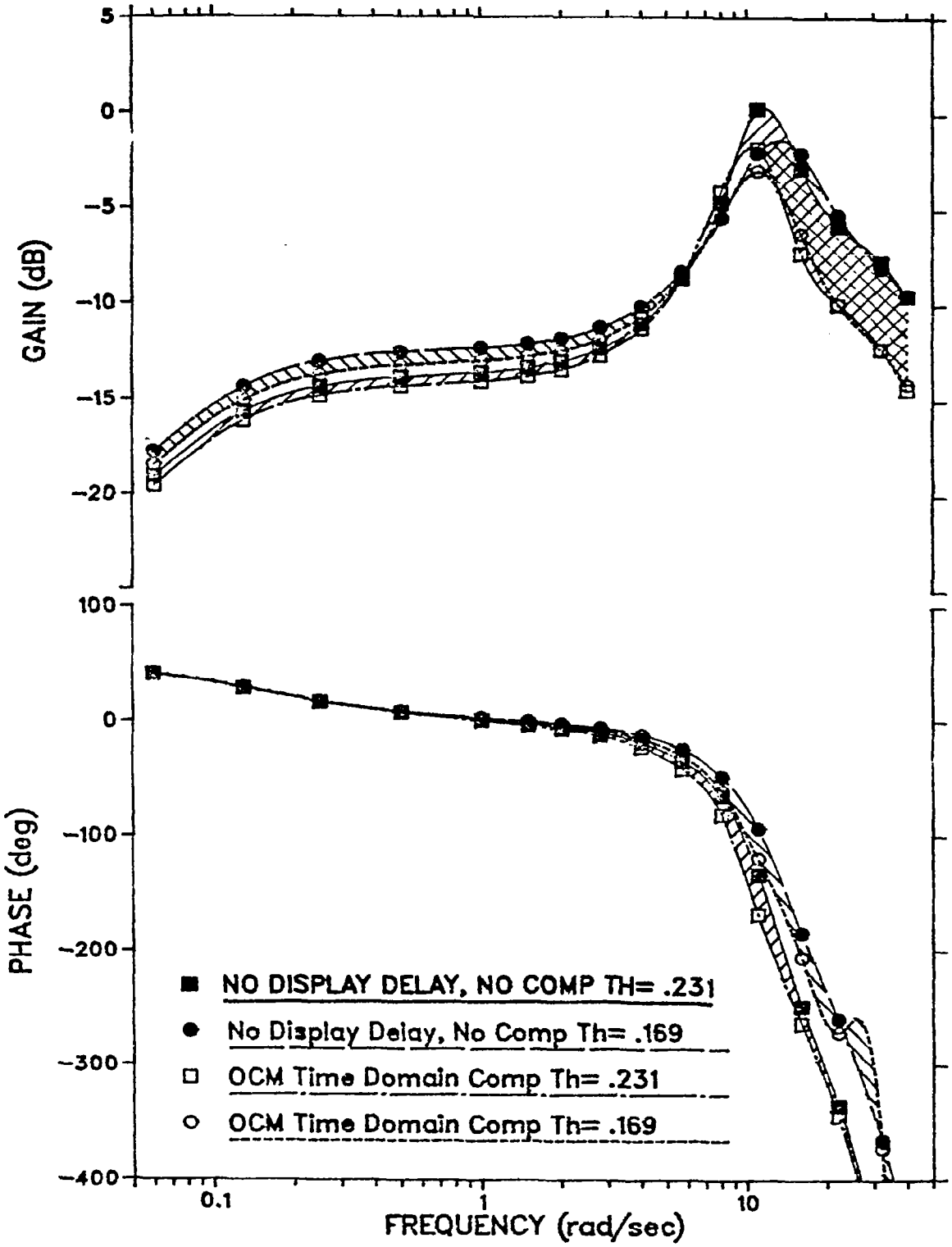

FIGURE 5.12: Sensitivity of OCM Time Domain Compensator to τ_H Variations — Pilot Describing Function

approximately a 1.3 dB error, whereas for T_N=.12, only a .7 dB error results. Considering that a 1 dB error was observed for the nominal pilot bandwidth (T_N=.1), this seems quite good and suggests that the design based on nominal T_N is quite robust with respect to changes in that parameter. Similar comments apply to the phase curves. Over the frequency band 6 to 11 rad/sec, the phase errors are almost twice the magnitude of those found for the "tuned" condition, but they are still less than the differences that would have occurred between the no-delay and full-delay conditions.

The sensitivity to variations in human time delay are illustrated in Figure 5.12. A comparison of this Figure with Figure 5.5 reveals, again, that differences between no-delay and compensated conditions with the pilot not matched exactly to the compensator design parameters are not significantly greater than those for the case where the parameters are identical. Gain differences are slightly larger (~.2 dB) for τ_H=.169 sec. Phase differences (around 10 rad/s) are more pronounced for τ_H=.23s, with approximately 4-8° of additional error over the τ_H=.169/case. The low peak in the phase at 12 rad/sec for the compensator with τ_H=.169 should be disregarded as this was due to an arbitrary plotting requirement to form a spline fit to the data rather than a smooth fit.

In summary, the compensator design seems quite robust to changes in parameters of the OCM that reflect individual differences among pilots. Variations in performance resulting from these changes are small, especially in comparison to an alternative of no compensation. The differences observed in the pilot describing functions are of the same order of magnitude as the basic compensator-no-delay differences with matched parameters. These results indicate that the compensator design should not have to be tuned to individual pilots which is, of course, an important practical consideration.

5.5 Application of OCM Time Domain Compensator to RSRA Hover Task

The OCM time-domain compensator for the RSRA hover task was designed using the procedure outlined at the end of Section 4.4 The fixed-base simulation was considered and the formulation of the problem was identical to that given in Chapter 3. Six noise equalization factors had to be determined corresponding to the three position and three attitude inputs to the CGI. It took four iterations with the OCM to find scale factors which gave good agreement with the no-delay performance. The values for these scale factors are listed in Table 5.5. Note that all but one of the factors is greater than one. This reflects the fact that the compensator, with $\underline{K}=\underline{I}$, improves performance to a greater extent than desired.

The rms scores for all state and control variables of interest are compared in Table 5.6 for the no-delay, full-delay and compensated conditions. The results for the uncompensated cases are identical to those given in Table 3.5, except derivative state variables are included here for completeness of comparison. The numbers shown in parentheses in the two columns for the conditions with delay show the percentage change in the quantities from the no-delay values.

The OCM time-domain compensator works remarkably well in restoring the various scores to their nominal, no-delay values. With the exception of the q and p variables all scores are less than five percent deviant from the no-delay case whereas the uncompensated deviations range up to thirty-one percent. The larger deviations in the q and p variables may well be an artifact of the trick used to determine predicted rates for the analysis. Even if these deviations were correct they are unlikely to diminish the overall utility of the compensator. The average deviation across all listed state-variable scores in the compensated case is 4.Ø percent as compared to 19.1 percent for no compensation. For the control variables, the average deviation from the no delay case of the compensated condition is 2.5 percent, as compared with 4.4 percent for the uncompensated case. Finally, the deviation in the performance metric J is only Ø.6 percent for the compensated

Table 5.5 Noise Equalization Factors for RSRA Hover Task

Variable	Noise Equalization Factor
x	1.37
y	1.07
z	1.00
θ	1.233
ϕ	1.12
ψ	.88

Table 5.6. Computed RMS Error Scores Vs. Delay Condition - RSRA

Variable \ Condition	No Display Delay, No Compensation	Full Display Delay, No Compensation	OCM Time Domain Compensation
Outputs			
x (ft)	8.47	9.87 (16.5%)	8.19 (3.4%)
$\dot{x}$ (ft/s)	1.58	1.84 (16.4%)	1.58 (0%)
y (ft)	7.48	9.57 (27.9%)	7.56 (1.0%)
$\dot{y}$ (ft/s)	1.43	1.83 (27.9%)	1.41 (1.4%)
z (ft)	3.86	4.49 (16.3%)	4.06 (5.2%)
$\dot{z}$ (ft/s)	1.28	1.44 (12.5%)	1.32 (3.1%)
θ (deg)	1.53	1.75 (14.4%)	1.53 (0%)
q (deg)	1.62	1.74 (7.4%)	1.87 (15.4%)
ϕ (deg)	1.43	1.79 (25.2%)	1.47 (2.8%)
p (deg)	2.37	2.65 (11.8%)	2.14 (10.7%)
ψ (deg)	0.99	1.29 (30.3%)	0.97 (2.1%)
R (deg)	0.86	1.06 (23.2%)	0.83 (3.6%)
Controls			
X_{long} (%)	3.73	4.05 (8.6%)	3.56 (4.8%)
X_C (%)	2.38	2.38 (0%)	2.35 (1.3%)
X_{lat} (%)	2.25	2.30 (2.3%)	2.20 (2.3%)
X_r (%)		7.86 (6.5%)	7.26 (1.7%)
J (Total Cost)	56.68	74.26 (31.0%)	57.03 (0.6%)

condition compared to thirty-one percent for no compensation. Inasmuch as the observation noise/signal ratio is assumed to be the same for the compensated and no-delay cases, this last comparison suggests that workload may be virtually restored to the desired level by the OCM time-domain compensator.

For the MIMO problem, pilot describing functions are difficult to measure and interpret. Here, we include predictions for some of the (unmeasurable) multiple internal describing functions defined earlier in Eq. (2.20). Several such describing functions (three for longitudinal control and three for lateral control) are shown in Figure 5.13. Plots are presented for the no-delay, full-delay and compensated conditions. It can be seen that the full-delay, no compensation cases generally have less phase lag (more lead) than the no-delay cases, as might be expected. The compensated cases sometimes require more lead at low frequencies but, with one exception δ_{LON}/θ require less lead at mid to high frequencies. The gain curves for the compensated cases depart more from the no-delay case than do those for the uncompensated condition. However, deviations in the main frequency band of interest are generally small.

In sum, these describing functions further indicate the compensator may provide some possible reduction in overall workload

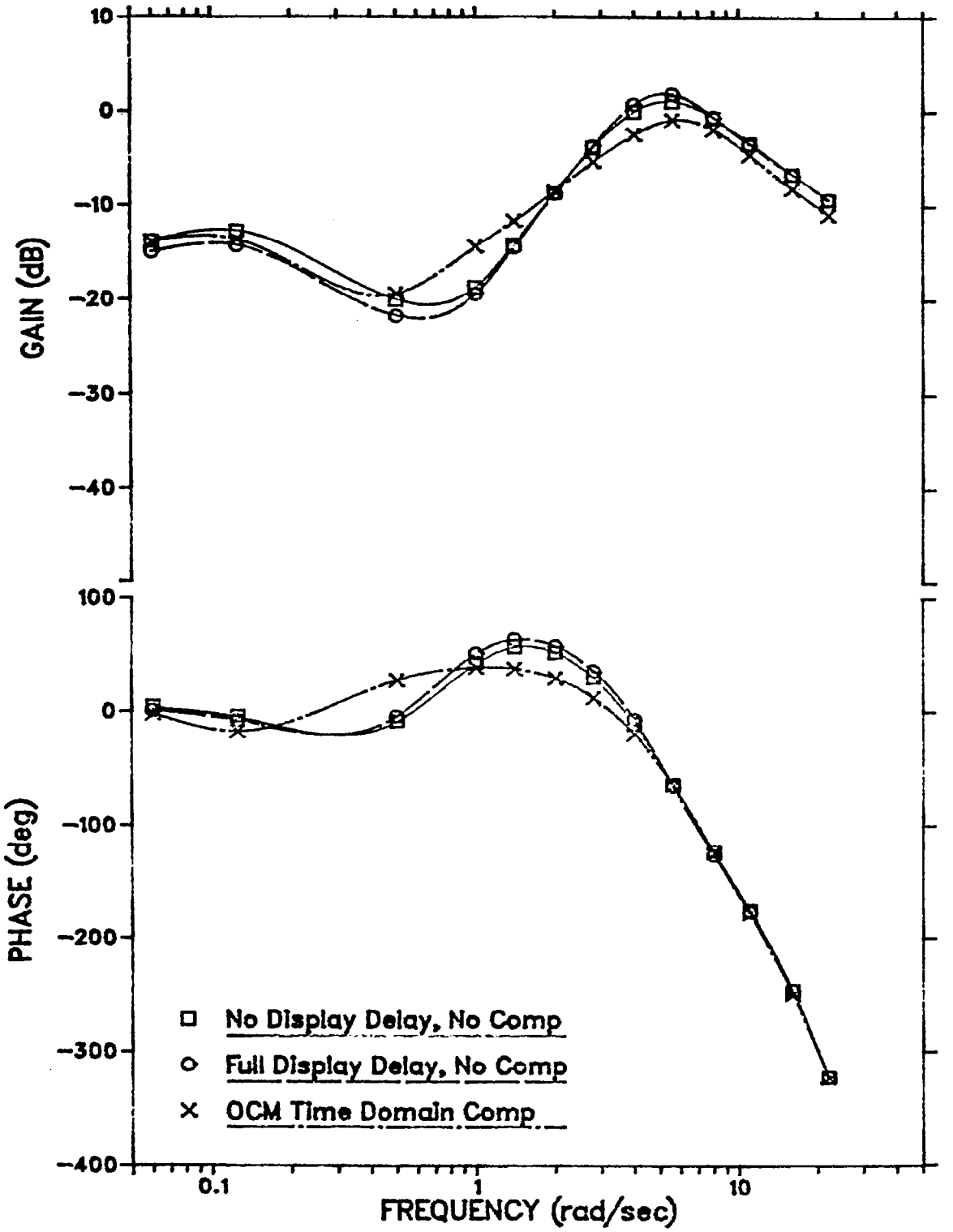

FIGURE 5.13a: Effect of Compensator on Pilot Multiple Internal Describing Function δ_{LON}/x (RSRA Task)

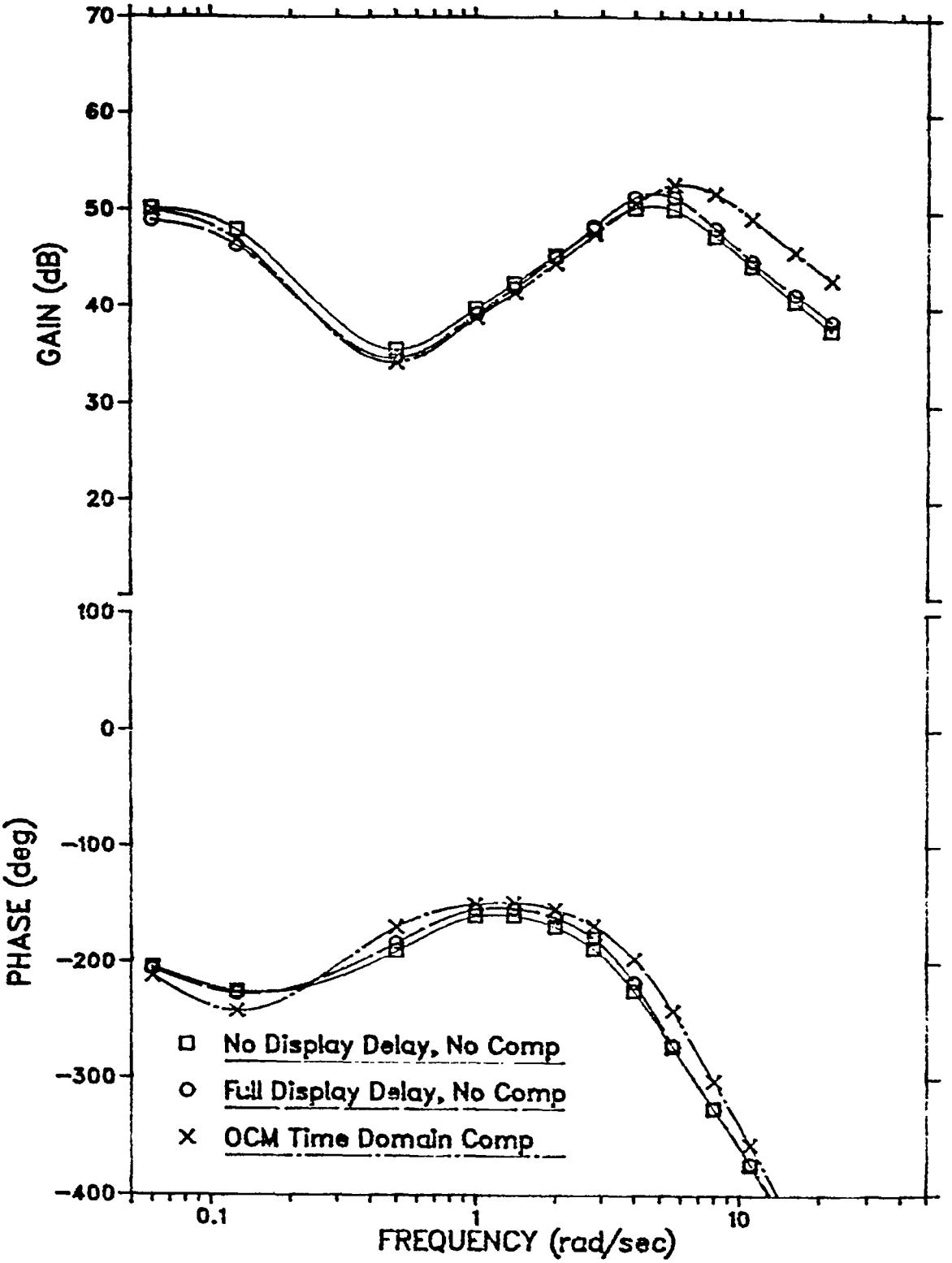

FIGURE 5.13b: Effect of Compensator on Pilot Multiple Internal Describing Function δ_{LON}/θ (RSRA Task)

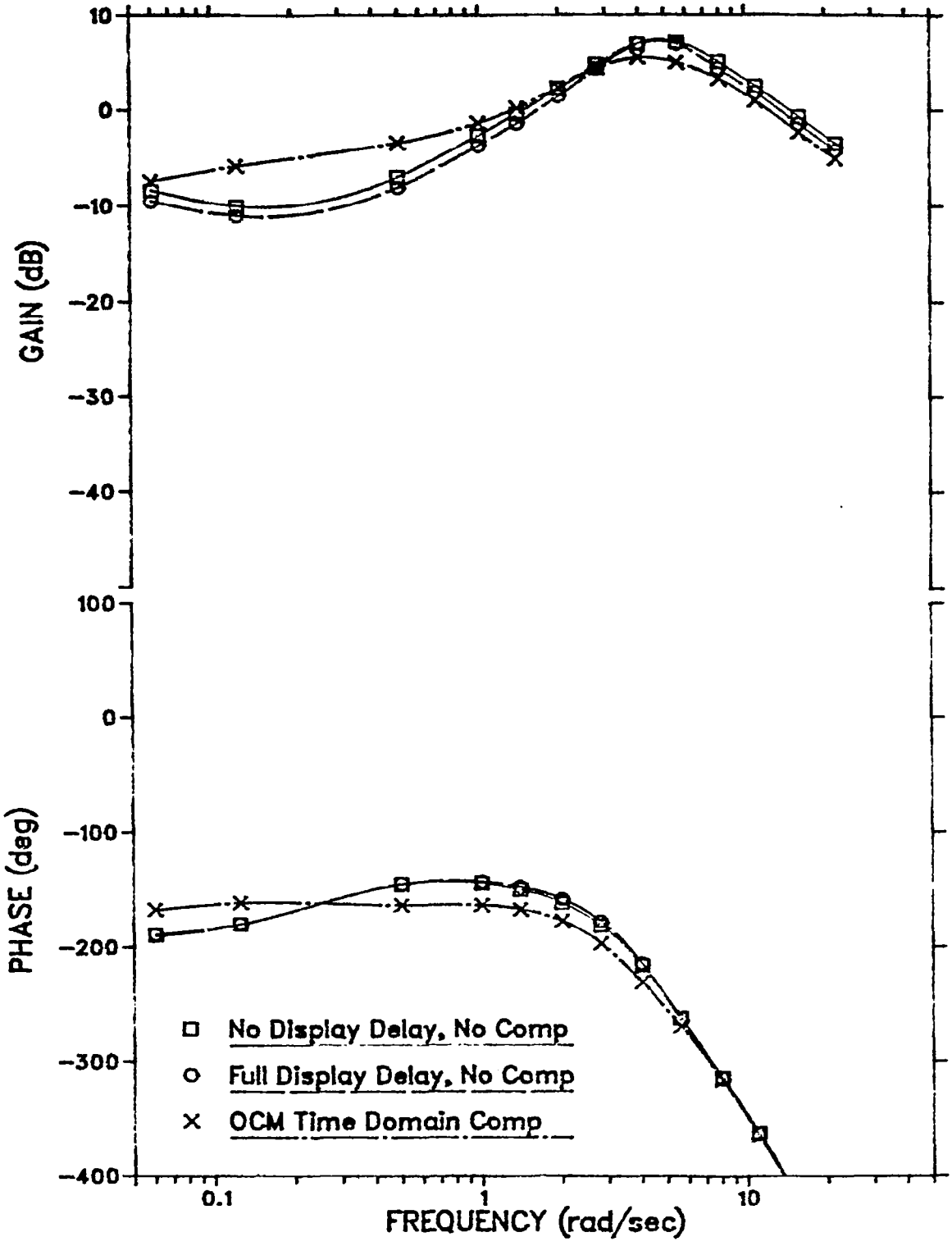

FIGURE 5.13c: Effect of Compensator on Pilot Multiple Internal Describing Function δ_c/z (RSRA Task)

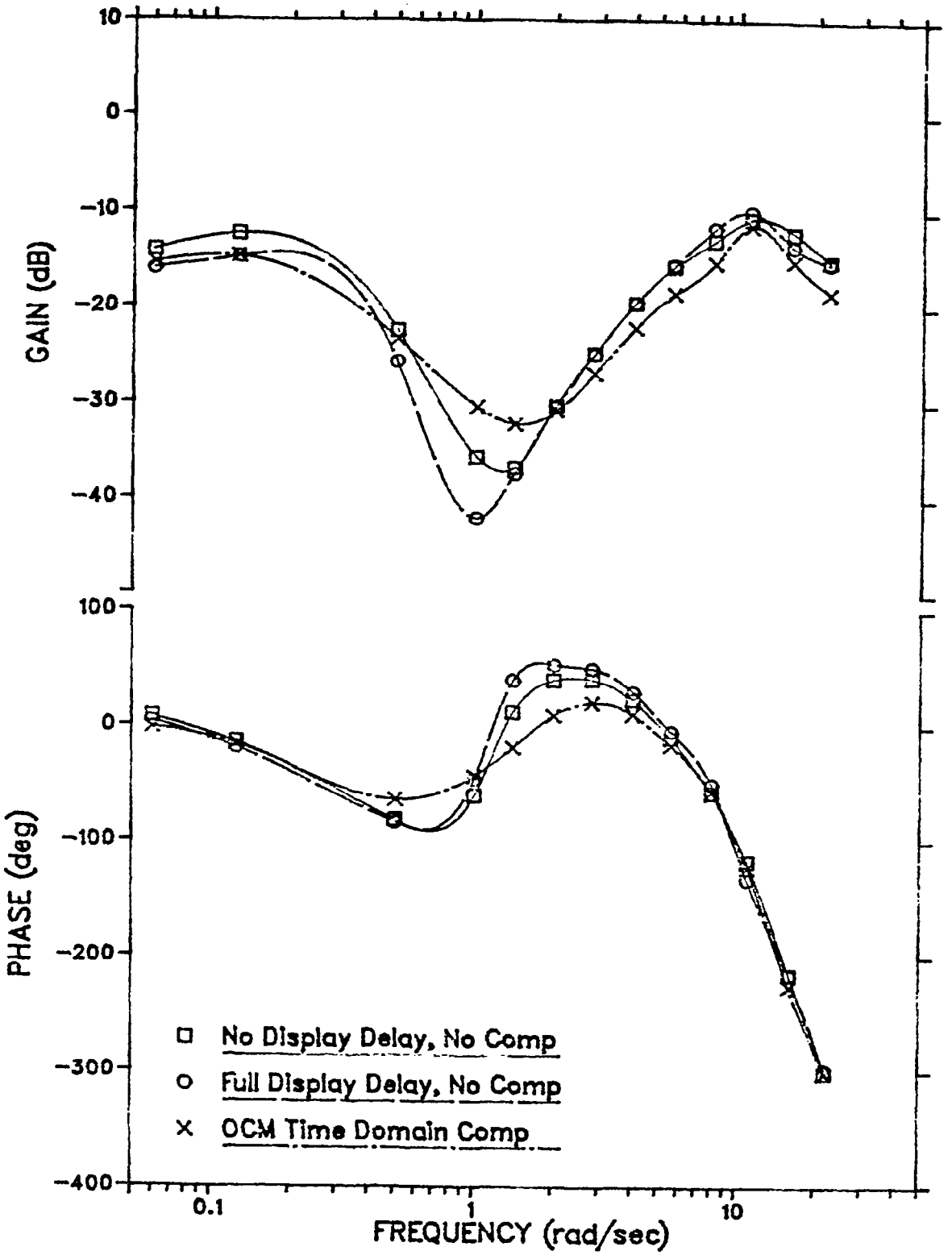

FIGURE 5.13d: Effect of Compensator on Pilot Multiple Internal Describing Function δ_{LAT}/y (RSRA Task)

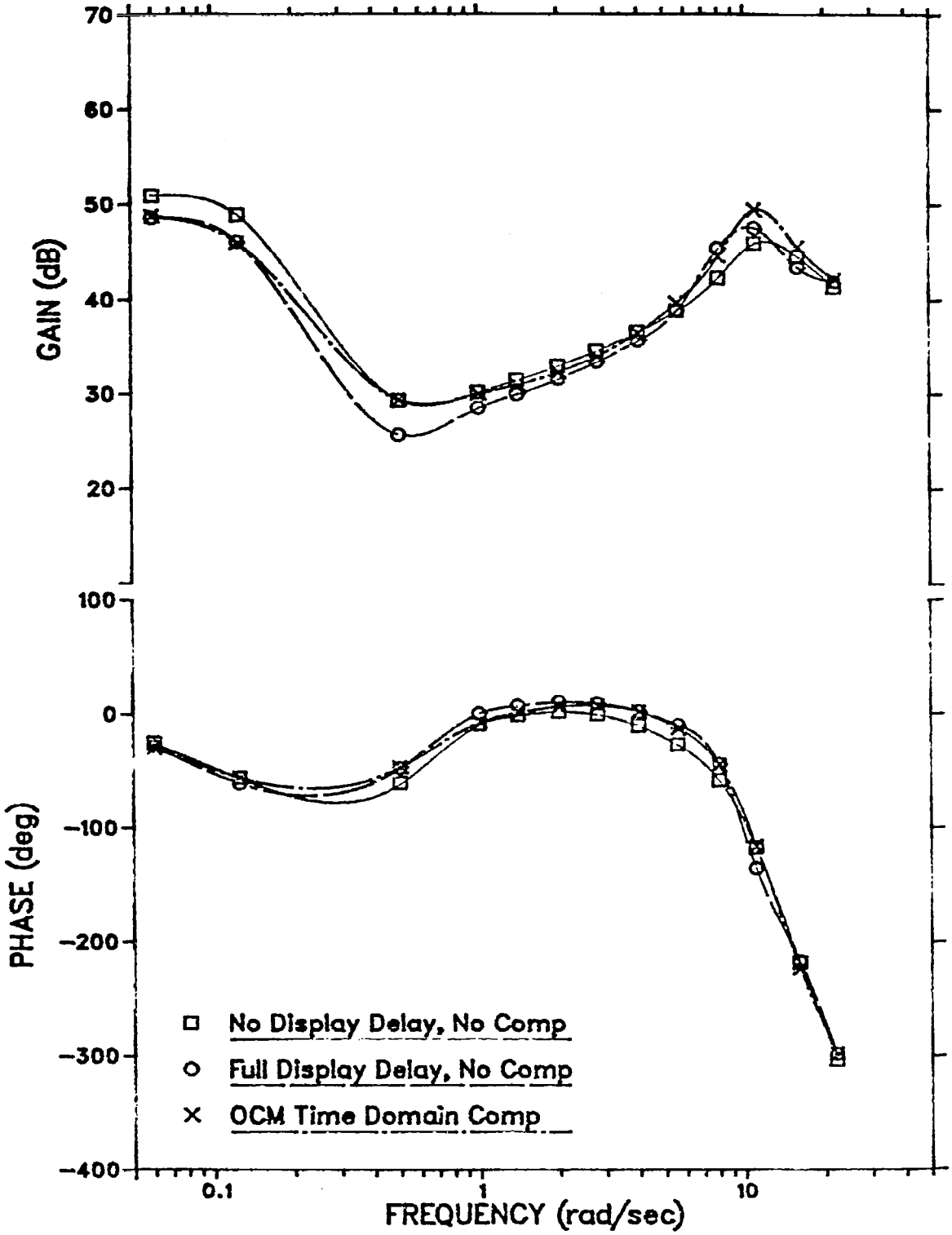

FIGURE 5.13e: Effect of Compensator on Pilot Multiple Internal Describing Function δ_{LAT}/ϕ (RSRA Task)

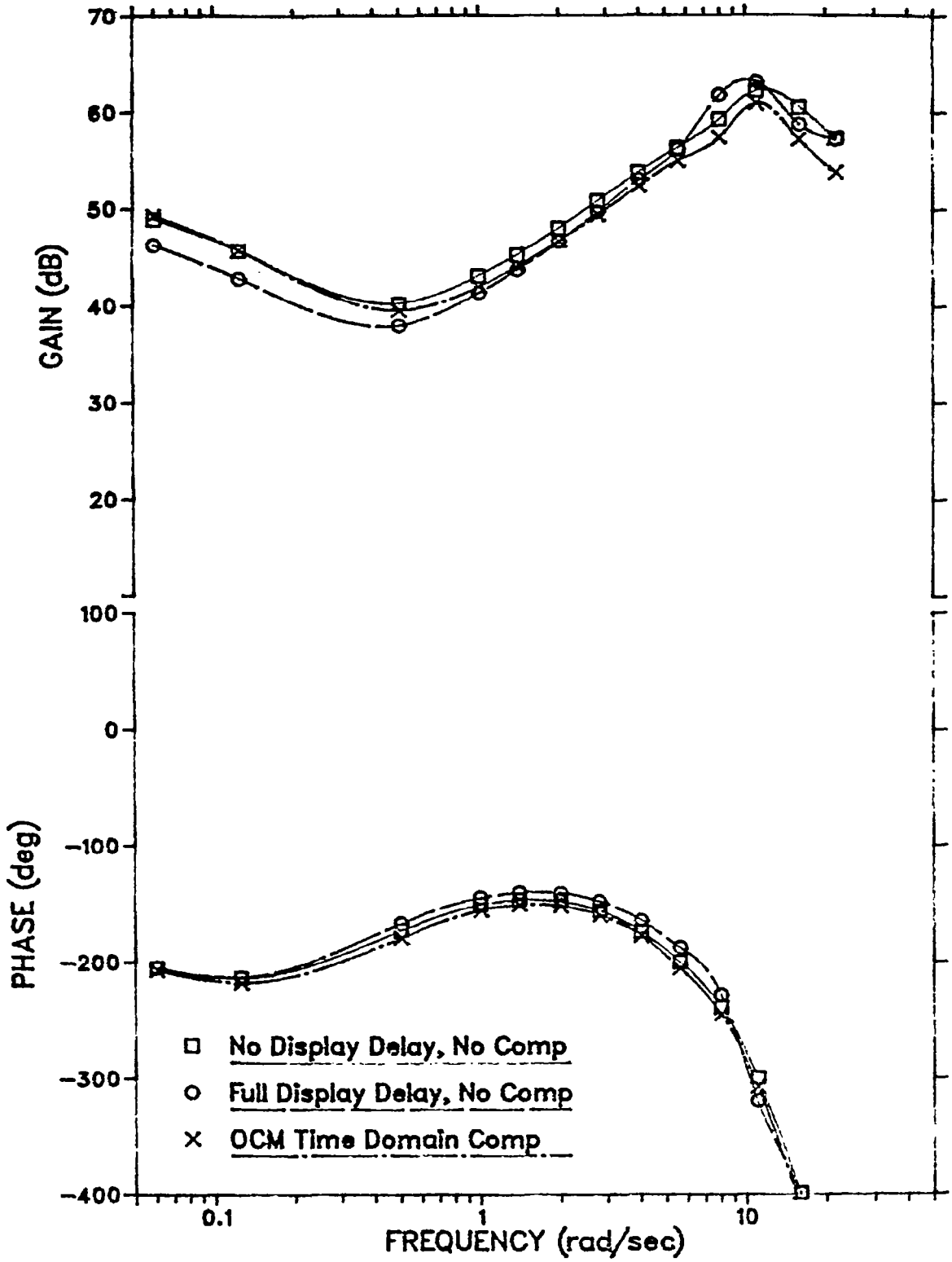

FIGURE 5.13f: Effect of Compensator on Pilot Multiple Internal Describing Function δ_r/ψ (RSRA Task)

from the uncompensated case.* The gain functions suggest slightly different strategies resulting from the compensator but it is difficult, if not impossible, to assess the significance of these differences in a purely analytic fashion (i.e., without experimental data).

* There is no theory for how to combine leads in the multivariable case to obtain an overall measure of workload.

6. CONCLUDING REMARKS

The Optimal Control Model (OCM) for pilot-vehicle analysis was used to analyze the effects of delay on closed-loop system performance and workload in a single-axis roll tracking task and in a multi-input, multi-output RSRA hover task. The single-axis results were compared with experimental data obtained in a similar, but not identical, problem situation. The comparison showed the OCM could, indeed, predict the effects of delays on performance and on a measure of pilot workload. The predictions for the RSRA task showed that even the relatively short delays associated with contemporary CGI systems could degrade hover performance and/or impose added workload to a significant degree. An interesting sidelight of the study was that the model results indicate that adding a motion platform would allow the pilot to attain performance/workload levels in the delayed situation that are comparable to these that could be achieved in a fixed-base, no-delay simulation.

The OCM was then used in the design and evaluation of three delay compensators. The compensators were evaluated from a pilot-centered orientation; i.e., the design criteria were chosen so that the objective of compensation was to restore, as closely as possible,the pilot's response to that of the no-delay situation.

All the compensators used were found to provide an improvement in performance and workload over full-delay, no compensation results in the single axis task. The best results were obtained for an OCM-based time domain compensator and, fortunately, this compensator is readily extended to multivariable problems. The time-domain compensator was then applied to the hover problem with extremely encouraging results. Performance scores were generally restored to within five percent of their no-delay values (most were much closer than this) whereas the uncompensated state-related scores were an average of about 20% higher than the no-delay values.

Thus, the OCM appears to be potentially very useful both for analyzing delay effects and for compensating for them, especially in multi-input/multi-output (MIMO) problems. There are, nonetheless, important questions and research issues remaining to be resolved.

The most important extension of this work is to conduct a thorough empirical validation of the model results. This should be done first in the single-axis context so that detailed predictions and subjective evaluations can be checked in a problem in which measurement and interpretation is relatively straightforward. Then, a more complex MIMO problem such as the RSRA hover problem, should be tested to assure that the results do generalize. It will

be important to obtain subjective pilot opinion in these studies in addition to objective measures.

Several other areas of investigation seem of interest. The simulation delay problem was analyzed here using essentially continuous models, but today's simulations are almost always discrete. It is certainly possible to design discrete compensators along the same lines employed herein and to use a modified OCM analyses to tune and evaluate the designs. In addition, we have studied only a linearized problem whereas most simulations are nonlinear. This is, of course, a well-established method of control analysis; however, some investigation of the utility of compensators based on linearization should be explored.

Finally, there are two areas of investigation that were not explored here because of lack of resources but would appear to involve only slight extensions of the effort. One is to consider delay compensation for the case where the motion platform is included in the simulation and the other, related area, is the consideration of different delays for different display variables.

REFERENCES

1. Baron, S., D.L. Kleinman, D.C. Miller, W.H. Levison and J.I. Elkind, "Application of Optimal Control Theory to the Prediction of Human Performance in a Complex Task", Wright Patterson Air Force Base, AFFDL-TR-69-81, March 1970.

2. Baron, S., R. Lancraft and G. Zacharias, "Pilot/Vehicle Model Analysis of Visual and Motion Cue Requirements in Flight Simulation", NASA CR-3312, October 1980.

3. Baron, S. and W.H. Levison, "The Optimal Control Model: Status and Future Directions", Proc. of International Conference on Cybernetics and Society, Cambridge, MA, October 1980.

4. Baron, S., R. Muralidharan and D.L. Kleinman, "Closed Loop Models for Analyzing Engineering Requirements for Simulators", NASA CR-2965, February 1980.

5. Chalk, C.R., T.P. Neal, T.M. Harris, F.E. Pritchard and R.J. Woodcock, "Background Information and User Guide for MIL-F-8785B(ASG), Military Specification - Flying Qualities of Piloted Airplanes", Air Force Flight Dynamics Laboratory Report AFFDL-TR-69-72, Wright Patterson Air Force Base, Ohio, August 1969.

6. Crane, D.F., "Time Delays in Flight Simulator Visual Displays", Proceedings 1980 Summer Computer Simulation Conference, Seattle, WA.

7. Crane, D.F., "Flight Simulator Visual-Display Delay Compensation", Winter Simulation Conference, Atlanta, GA, December 1981.

8. Hess, R.A., "Analytical Display Design for Flight Tasks Conducted Under Instrument Meteorological Conditions", IEEE Trans. on Systems, Man and Cybernetics, SMC-7, No. 6, June 1977.

9. Hoffman, W.C., D.L. Kleinman and L. Young, "Display/Control Requirements for Automated VTOL Aircraft", ASI-TR-76-39-, October 1976.

10. Kleinman, D.L., "Solving the Optimal Allocation Problem in Manual Control", IEEE Trans. on Automatic Control, AC-21, 1976.

11. Kleinman, D.L., S. Baron and W.H. Levison, "A Control Theoretic Approach to Manned-Vehicle Systems Analysis", IEEE Trans. on Auto. Control, Vol. AC-16, No. 6, December 1971.

12. Levison, W.H., "A Model Based Technique for the Design of Flight Directors", Proc. of Ninth Annual Conference on Manual Control, MIT, Cambridge, MA, May 1973.

13. Levison, W.H., "Motion Cueing for Flight Simulators", Report No. 4154, Bolt Beranek and Newman, Inc., Cambridge, MA, July 1979.

14. Levison, W.H., J.I. Elkind and J.L. Ward, "Studies of Multi-Variable Manual Control Systems" A Model for Task Interference", NASA CR-1746, May 1971.

15. Queijo, M.J. and D.R. Riley, "Fixed-Base Simulator Study of the Effect of Time Delays in Visual Cues on Pilot Tracking Performance", NASA TN D-8001, October 1975.

16. Ricard, G.L. and W.T. Harris, "Lead/Lag Dynamics to Compensate for Display Delays", Journal of Aircraft, Vol. 17, No. 3, 1980.

17. Sage, A. and J. Melsa, "Estimation Theory with Applications to Communication and Control", McGraw-Hill, 1971.

1. Report No.	2. Government Accession No.	3. Recipient's Catalog No.
NASA CR-3604		

4. Title and Subtitle	5. Report Date
AN OPTIMAL CONTROL MODEL APPROACH TO THE DESIGN OF COMPENSATORS FOR SIMULATOR DELAY	OCTOBER 1982
	6. Performing Organization Code

7. Author(s)	8. Performing Organization Report No.
S. Baron, R. Lancraft, and A. Caglayan	BBN 5004
	10. Work Unit No. T5232

9. Performing Organization Name and Address	11. Contract or Grant No.
Bolt Beranek and Newman, Inc., 50 Moulton Street Cambridge, Massachusetts 02238	NAS2-10907
	13. Type of Report and Period Covered Contractor Report

12. Sponsoring Agency Name and Address	14. Sponsoring Agency Code
National Aeronautics and Space Administration Washington, DC 20546	505-55-31

15. Supplementary Notes

Final Report.
Ames Technical Monitor: D. F. Crane, Mail Stop: N243-9, Moffett Field, CA 94035, (415) 965-5324, FTS 448-5324.

16. Abstract

This report summarizes an analytical study of the effects of display delay on pilot performance and workload and of the design of filters to ameliorate these effects. The Optimal Control Model for pilot/vehicle analysis was used both to determine the potential delay effects and to design the compensators. The model was applied to a simple roll tracking task and to a complex hover task. The results confirm that even small delays can degrade performance and impose a workload penalty. A time-domain compensator designed by using the Optimal Control Model directly appears capable of providing extensive compensation for these effects even in multi-input, multi-output problems.

17. Key Words (Suggested by Author(s))	18. Distribution Statement
Flight Simulation	Unclassified - Unlimited Subject Category 05

19. Security Classif. (of this report)	20. Security Classif. (of this page)	21. No. of Pages	22. Price
Unclassified	Unclassified	111	A06

For sale by the National Technical Information Service, Springfield, Virginia 22161

NASA-Langley, 1982